



OPEN ACCESS

EDITED BY

Magdalena Scheck-Wenderoth,
GFZ German Research Centre for
Geosciences, Germany

REVIEWED BY

Antonio Caracausi,
National Institute of Geophysics and
Volcanology, Italy
Maria Francesca Ferrario,
University of Insubria, Italy

*CORRESPONDENCE

Carolina Canora,
✉ carolina.canora@uam.es

SPECIALTY SECTION

This article was submitted to Structural
Geology and Tectonics,
a section of the journal
Frontiers in Earth Science

RECEIVED 03 October 2022

ACCEPTED 27 January 2023

PUBLISHED 09 February 2023

CITATION

Canora C, Cuevas Rodríguez J,
Martínez Díaz JJ and Garralón A (2023),
Analysis of a travertine system controlled
by the transpressional activity of the
Alhama de Murcia fault: The Carraclaca
site, eastern Betic Cordillera, Spain.
Front. Earth Sci. 11:1060363.
doi: 10.3389/feart.2023.1060363

COPYRIGHT

© 2023 Canora, Cuevas Rodríguez,
Martínez Díaz and Garralón. This is an
open-access article distributed under the
terms of the [Creative Commons
Attribution License \(CC BY\)](https://creativecommons.org/licenses/by/4.0/). The use,
distribution or reproduction in other
forums is permitted, provided the original
author(s) and the copyright owner(s) are
credited and that the original publication in
this journal is cited, in accordance with
accepted academic practice. No use,
distribution or reproduction is permitted
which does not comply with these terms.

Analysis of a travertine system controlled by the transpressional activity of the Alhama de Murcia fault: The Carraclaca site, eastern Betic Cordillera, Spain

Carolina Canora^{1*}, Jaime Cuevas Rodríguez¹,
José Jesús Martínez Díaz^{2,3} and Antonio Garralón⁴

¹Dpto. Geología y Geoquímica, Facultad de Ciencias, Universidad Autónoma de Madrid, Madrid, Spain, ²Dpto. Geodinámica, Estratigrafía y Paleontología, Facultad de Geología, Universidad Complutense de Madrid, Madrid, Spain, ³Instituto de Geociencias, Consejo Superior de Investigaciones Científicas y Universidad Complutense de Madrid, Madrid, Spain, ⁴Dpto. Medio Ambiente, Centro de Investigaciones Energéticas, Madrid, Spain

Continental carbonates, such as travertines and tufas, formed from CO₂-rich groundwater degassing as it emerges at the Earth's surface, are often associated with major crustal-scale faults. The Carraclaca site, in the Lorca-Totana section of the Alhama de Murcia Fault, Spain, presents a complex geomorphological landscape controlled by active tectonics. The geology here records the interaction between Quaternary alluvial fans, travertines, and a pop-up structure developed in a transpressional section of the fault. The Alhama de Murcia Fault is an 80 km long left-lateral strike-slip fault that is one of the main seismogenic structures in the Iberian Peninsula. In this work, we examined the relation between travertine precipitation in the Carraclaca site and the tectonic activity of this fault zone through morphological and geochemical studies. The $\delta^{13}\text{C}$ and $\delta^{18}\text{O}$ isotopic signals indicate that the carbonate deposits are hydrothermal. In addition, the $^{87}\text{Sr}/^{86}\text{Sr}$ ratios in the samples suggest subsurface fluid interaction with the Miocene sediments and the Alpujárride basement, located below the alluvial deposits. Tectonic activity in the Alhama de Murcia Fault might generate the opening of deep water circulation in the crust every time a seismic event occurs, giving rise to hydrothermally derived carbonates precipitation. Deep waters rise and reach the surface interacting with meteoric waters, resulting in travertine formation. Therefore, the Carraclaca carbonate deposits study can inform us about the seismogenic cycle of the fault in the Lorca-Totana section.

KEYWORDS

travertine, stable isotopes, paleoseismometer, Alhama de Murcia fault, transpressional fault, geochemistry

1 Introduction

The study of travertine associated with fault activity has been the subject of several research studies (Hancock et al., 1999; Pentecost, 2005; Andrews, 2006; Uysal et al., 2007; 2009; Zentmyer et al., 2008; Pedley, 2009; Ascione et al., 2013; Özkul et al., 2013; 2014; Brogi et al., 2014; 2016; Gradziński et al., 2014; Mason et al., 2017). Travertine precipitation occurs in the presence of CO₂ dissolved in groundwater, and is a good indicator of fault-controlled hydrologic systems. Some travertine characteristics such as location, shape, or age provide

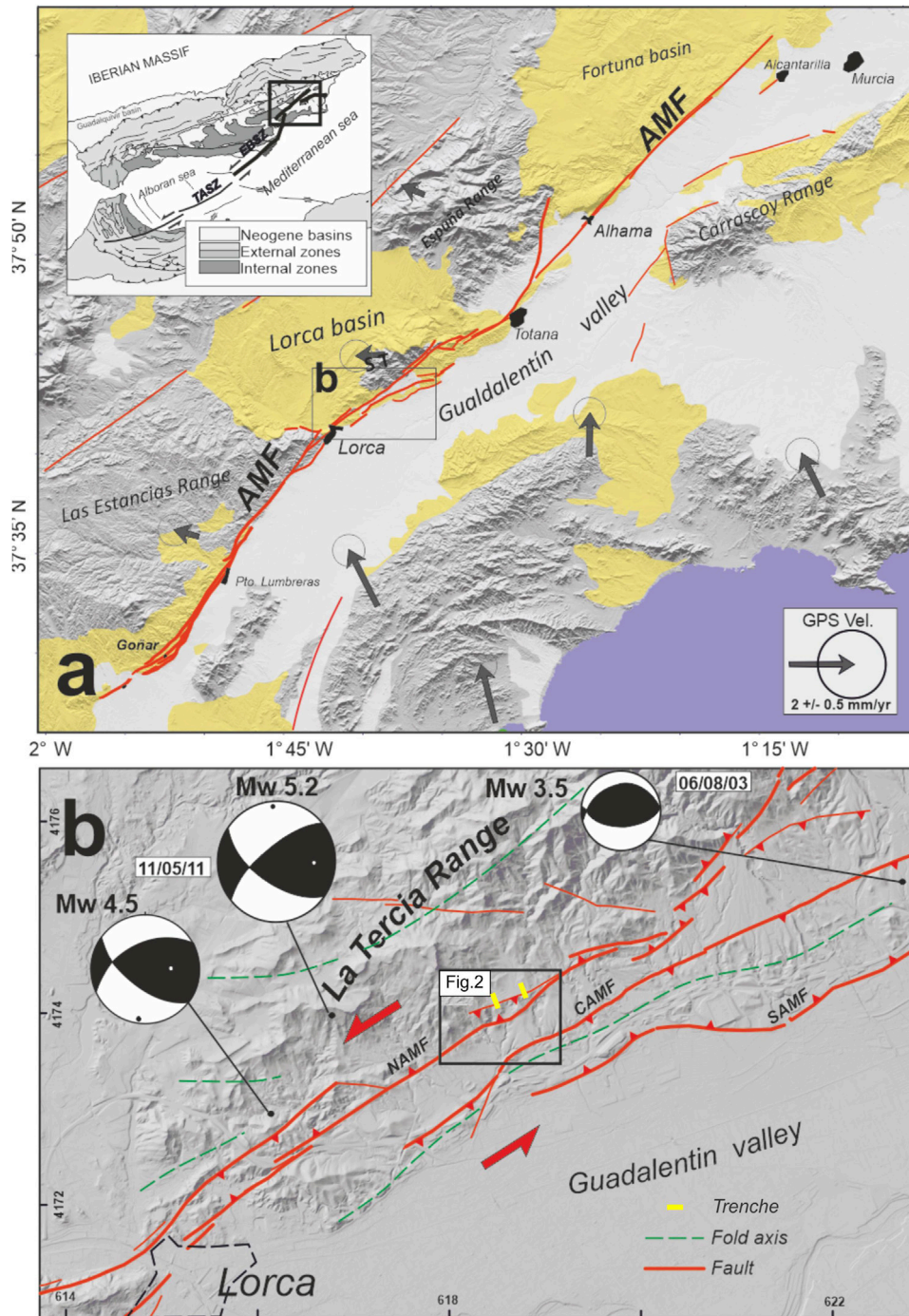


FIGURE 1
 Location map of the study area in the eastern sector of the Trans-Alboran Shear Zone (TASZ). **(A)** Alhama de Murcia Fault trace (AMF). The fault limits the Neogene basins (yellow zones) and the mountain ranges of La Tercia, Sierra Espuña and Las Estancias to the northwest and the Quaternary Guadalentín Valley (white zones) to the southeast. GPS velocities from CuaTeNeo network in eastern Betics calculated by Echevarria et al., 2013 considering the Iberian massif fixed. **(B)** Digital elevation model of the Lorca-Totana section of the AMF with the latest seismic series occurring in the area. NAMF, North Alhama de Murcia Fault; CAMF, Central Alhama de Murcia Fault; SAMF, South Alhama de Murcia Fault. The inset shows the Carraclaca study area in Figure 2.

information about the faults and fractures that trigger fluid circulation, especially concerning structural patterns and the permeability (Altunel and Hancock 1993a; b; Faccenna et al., 1993; Hancock et al., 1999; Martínez-Díaz and Hernández-Enrile 2001; Brogi and Capezzuoli 2009; Temiz and Eikenberg 2011). In most of cases, travertine deposits are associated with normal faults. Few studies

have focused on travertines associated with strike-slip faults (Faccenna et al., 2008; Brogi et al., 2012; Colak et al., 2012; 2015; De Filippis et al., 2013; Temiz et al., 2013).

Some paleoseismic studies carried out in regions having moderate to high seismicity used travertine and speleothem dating for seismic event identification taking advantage of its cyclical nature of

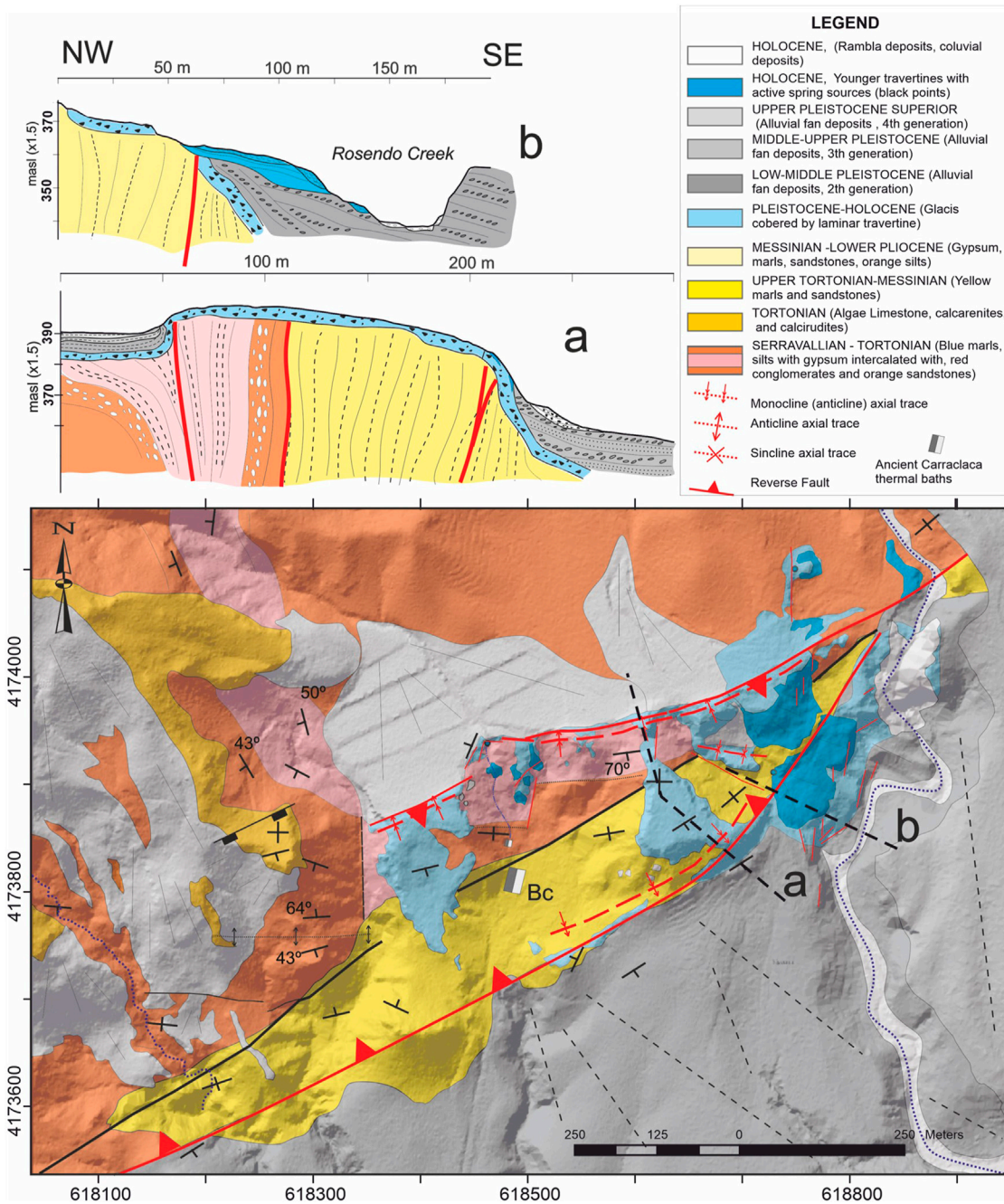


FIGURE 2 Geological-structural map of the Carralaca area showing main fault traces and travertine deposits and related geological cross sections through the pop-up structure.

precipitation (Hancock et al., 1999; Gilli, 2005; Shi et al., 2014; Selim et al., 2016). Hancock et al. (1999) use travertine deposits related with active fault considering their morphology, location, and deformation. They use the term “travtonics” for the study of the tectonic implications of those carbonate deposits. Geochemical analyses performed on travertine associated with structural features suggest that CO₂-rich deep water travels to the surface through faults and fractures (Zentmyer et al., 2008) since these are the pathways for hydrothermal fluids to rise (Sibson 1990). These carbonate deposits are called thermogenic travertines (Pentecost, 2005), and are excellent

indicators of the tectonic activity pattern in hydrothermal environments. The process would be as follows: acidic water that has dissolved the carbonate parent rock at depth travels to the surface where it degasses, producing travertine precipitation. The activity of the faults, due to their episodic character, gives rise to different precipitation cycles of CaCO₃. Therefore, it is feasible to detect deposition sequences associated with their recurrence. Knowing the geochemistry, morphology, structure, and age of each precipitation episode is the clue to comprehending the nature of these travertine deposits and its possible relation with the seismic cycle of faults.

In this study, we analyze the Carraclaca travertine deposits (Figures 1, 2), at the La Tercia Range Mountain front, along the NW edge of the Guadalentín Tectonic Depression. The travertine outcrop is along the trace of the northern branch of the Alhama de Murcia Fault (AMF), one of the three main strands in this section of the fault. This study area represents a perfect scenario for establishing connections between active tectonics and hydrothermal systems through geological and geochemical analysis of travertines.

To date, paleoseismic studies through trench analysis have been the only carried out to determine seismic events in the Lorca-Totana segment of the AMF (Masana et al., 2004; Martínez-Díaz et al., 2012; Ortuño et al., 2012; Ferrater et al., 2016; Gómez-Novell, 2021). However, we still have no evidence of major paleoseismic events with surface rupture associated with the northern strand of the fault, this being the branch that controls the relief of the La Tercia Range (NAMF in Figure 1B).

The possibility that the travertine formation at Carraclaca is linked to the seismic cycle of the AMF (Martínez-Díaz and Hernández-Enrile, 2001) gives us the opportunity to use a new methodological approach to increase the knowledge of the earthquakes history of this fault during the Quaternary. This method, through geochemical study of the samples, may open a determining window not only for the knowledge of the AMF but also for other faults in the Iberian Peninsula that have associated travertine deposits, such as the Crevillente fault or the Jumilla fault, among others.

Herein, we describe the Carraclaca travertine deposits through their lithological and morphological types and the analysis of stable isotopes ($\delta^{13}\text{C}$ and $\delta^{18}\text{O}$) and Sr isotopes that have implications for fluid flow. Many authors have shown that stable isotope analyses help to understand the genesis of continental carbonate deposits such as travertines and tufas (Friedman, 1970; Manfra et al., 1974; Fouke et al., 2000; Pentecost, 2005; Kele et al., 2011; DeFilippis et al., 2013; Vignaroli et al., 2016). These analyses can indicate the precipitation conditions of the carbonates, the origin of the fluids that carry them in solution, and the carbon source through the study of the carbon and oxygen content. The $\delta^{13}\text{C}$ and the $\delta^{18}\text{O}$ ratios of carbonate samples have been used to classify travertine into thermogenic and meteorogenic and to characterize the origin of the parental fluids (Vignaroli et al., 2016). In thermogenic travertine, CO_2 comes from deep fluids that interact with carbonate rocks in the basement, while in meteorogenic travertine, it derives from surface reservoirs or from the atmosphere. The $\delta^{13}\text{C}$ values reflect the different sources of CO_2 . While thermogenic travertines have, in general, positive values (between -3‰ and $+8\text{‰}$), meteorogenic travertines have very negative ones (i.e., -8.48‰ according to Pentecost, 2005). We have also calculated the temperature of the source fluids that formed our travertines from the $\delta^{18}\text{O}$ values using the Kele et al. (2015) equation.

We conclude by proposing a conceptual model of the hydrological system that fed the spring of the travertine deposit.

2 Geological setting

Montenat first described the AMF in 1973. This is an 80 km long, NE-SW trending sinistral strike-slip fault with a reverse component. It is part of the Betic segment of the Trans-Alboran Shear Zone and it is located in the Eastern Betics Shear Zone (EBSZ) (De Larouzière et al., 1988) as one of the most active faults in the Iberian Peninsula (Figure 1A). The Eastern Betics formation is traced back to the Miocene when the oblique collision of Alboran and the South-

Iberian and Maghreb margins began (Balanyá and García-Dueñas, 1987; Lonergan and White, 1997; Faccenna et al., 2004; Booth-Rea et al., 2007). Between the Burdigalian and Tortonian a phase of upper crustal extension took place (Armijo 1977; Martínez-Martínez & Azañón 1997; Rodríguez-Fernández et al., 2012), exhuming basement rocks of the Alpujárride and Maláguide tectonic complexes and creating several marine basins of Neogene age (such as the Lorca basin). The extensional phase formed a set of NW-SE and NE-SW normal faults that were sealed by sedimentary deposits as extension stopped (Álvarez et al., 1989; Lonergan and Schreiber, 1993; Booth-Rea et al., 2004; 2012; Meijninger and Vissers, 2006). At the end of the Neogene, there was a tectonic inversion associated with the convergence between Africa and Europe, which gave rise to large transpressional zones such as the AMF. This convergence is still active and presents a rate of 4–6 mm/year (Argus et al., 1989; Fernandes et al., 2007; Serpelloni et al., 2007), it is absorbed in the Iberian margin by internal deformation and faults belonging to the EBSZ (Masana et al., 2004). The recent earthquakes in Totana (Mw 4.5) and Lorca (Mw 5.2) support the current transpressive character of the fault (Figure 1B). Echeverría et al. (2013) proposed a geodetic slip rate of 1.5 ± 0.3 mm/year for the AMF and Palomares fault together through geodetic analysis and strain modelling. From the analysis of paleoearthquakes associated with the AMF activity, the studies carried out have reflected the occurrence of surface rupture earthquakes of magnitudes up to 7.0 (Masana et al., 2004; Martínez-Díaz et al., 2012; Ortuño et al., 2012; Gomez-Novell, 2021).

Martínez-Díaz et al. (2012) divided the AMF into four sections according to its geometry, morphological expression, and seismicity (Figure 1A). The Goñar-Lorca is the southernmost section of the fault. It is characterized by very low seismicity. The general trend of this section is N40E, and it consists of a thin northern fault zone that divides into several branches to the south. The fault here acts as a boundary between the Guadalentín basin and the Las Estancias range. Ortuño et al. (2012), based on alluvial channel displacements and long-term geological data, assessed a slip rate of 1.6–1.7 mm/year for the past 200 ka. The Lorca-Totana is the next section to the north and the most studied segment of the AMF. Its three branches have an approximate orientation of N60E and limit La Tercia Range and the Guadalentín Valley to the SE and NW, respectively (Figure 1B). A geological slip rate of 0.8–1.55 mm/year has been calculated for this section through paleoseismic studies (Ferrater et al., 2016; Gómez-Novell, 2021). Along the Totana-Alhama section the fault recovers its N40E orientation. Here the fault has less morphological expression, with scarps under 1 m high, possibly because the Quaternary deposits cover it in part. This section also exhibits several strands, one of which borders the Espuña mountain range. So far, we have no information about the slip rate of this section. The northernmost is the N45E trending Alhama-Alcantarilla section. The AMF here has a diffuse geomorphic expression, which can be ascribed to the transfer of the deformation to the nearby Carrascoy fault. Herrero-Barbero et al. (2020) estimate a net-slip rate of about 0.32 mm/year in this section for the last 4.8–7.6 Ma, based on GPS convergence vectors and cross-section restorations.

3 Carraclaca site

The study area is located in the Lorca-Totana section of the AMF, where the deformation is distributed in several branches that produce a wide deformation area (Figures 1, 2). The northwest strand bounds

to the north with Sierra de la Tercia, the main mountain range in the area. Between the northwest and central branches, the fault movement forms a sinking area covered by Late Pleistocene alluvial fan deposits. The southern strand controls the position of the younger Holocene fans in the Guadalentín depression to the southeast (Martínez-Dí' and Hernandez, 2001; Silva et al., 1997). The deep structure of the AMF in this sector is not yet fully known, but it has been proposed that the central and southern branches connect at depth to the northern strand, that dips between 55° and 70° to the NW (Martínez-Díaz et al., 2012). The distribution of Pleistocene fans derived from the mountain range erosion and the hot spring travertine deposits has been controlled by the AMF activity (Martínez-Díaz and Hernández-Enrile, 2001; Martínez-Dí' and Hernandez, 2001; Martínez-Díaz et al., 2003; Masana et al., 2004).

The Carraclaca site is located on the northern branch of the fault, 5 km northeast of Lorca city (Figure 1). The Carraclaca spring outcrop was first described in detail by Armijo in 1977, who interpreted the site as a monoclinical fold affecting Quaternary deposits. According to Silva et al. (1997), this fold had a vertical coseismic slip between 0.2 and 0.8 m. These authors also described a surface rupture in the upper part of the fold structure. Later on, Martínez-Díaz and Hernández-Enrile (2001) evidenced the existence of travertine accumulations related to Pleistocene and Holocene water upwelling and linked to the neotectonic activity of the AMF. In the paper, the authors estimated a quaternary vertical slip rate of 0.087 mm/yr based on regional-scale uplift rates and U-Th dating.

The Carraclaca site has a pop-up structure generated by the uplift of the wedge block bounded by the northern branch of the main fault and a secondary fault (Figure 2). The faults here trend N60°E, and the coaxial component of the transpression creates a double monocline fold driven by the upward extrusion of the block that affects the recent deposits (Figure 2).

The Carraclaca pop-up affects a thin, hardened Lower Pleistocene surface derived from slope debris deposits, hereafter referred to as glacia, which is highly resistant to erosion. That preserves the monoclinical folding geometry and acts as a shield for the alluvial fans flowing from the northern range. These Pleistocene to Holocene alluvial fans result from the fault activity along the southern limit of the La Tercia Range. There were two phases of aggradation, one in the Middle Pleistocene followed by a second phase in the Late Pleistocene to Holocene (Silva et al., 1992; Silva, 1994; Martínez-Díaz et al., 2003). The inner part of the pop-up block consists of materials from two different Miocene formations separated by a non-active fault: blue marls, silt with gypsum, deltaic orange conglomerates, and sandstones from the Serravallian and Tortonian in the northern part, as well as yellow marls and sandstones from the Upper Tortonian to the south (Figure 2). Covering the previously described materials is the heavily cemented lower old Quaternary glacia that delineates the box fold and is the basement for the carbonate deposits that are the subject of this study. Despite the ductile nature of the materials forming the pop-up core, the box-shaped geometry, with a sub-horizontal flat top, suggests that the faults bounding the block continue at depth until they reach the rigid substrate (probably the Paleozoic metamorphic rocks). That forms a solid block between them, which can be extruded upwards by translation without significant internal folding.

In the Carraclaca area, there are several springs aligned with the fault planes located at the intersection with minor NNE-SSW and NW-SE fractures. There, the waters rise to the surface producing a square kilometer of travertine formations that cover the tectonic block

uplifted by the faults. Some travertines are deformed, following the monocline geometry (Figure 2).

4 Carraclaca travertines

The travertine deposits described in this study occur in the surroundings of the old thermal spring of Carraclaca, active until the last century (Figure 3). At present, the thermal pools are abandoned, possibly because of the low water flow from the current springs (0.3 L/s, according to Martínez and Moreno, 2005). This zone shows numerous water upwelling points at different heights, which may be related to the complexity of fracturing. Martínez-Díaz and Hernández-Enrile (2001) studied for the first time the relationship of the Carraclaca travertines with AMF activity by Th-U dating and petrographic analysis. These authors described four types of travertine deposit morphologies, following the classification made by Hancock et al. (1999). Terrace-mound and slope travertines, formed by downslope water runoff. Fissure-ridge travertines, filling fractures with multiple bands of crystalline material. Range-front travertines, deposited from water sources in the slope forming the monocline steeped flank tilted by main fault plane activity. And finally, eroded sheets travertines, formed by finely bedded and eroded layers of pure calcite covering other travertines. Martínez-Díaz and Hernández-Enrile (2001) obtained ages for four travertine samples ranging from 306 ka to 26 ka, indicating that travertine formation at Carraclaca has taken place since at least the Middle Pleistocene, and created a model for travertine formation.

To characterize Carraclaca's carbonate deposits, we have analyzed the travertine morphotypes and lithotypes present in the area, as well as the sedimentary structures. The travertine distribution consists of isolated patches overlying the Miocene deposits of the Lorca basin. Several depositional units composed of bedded travertines (Figure 4) form the carbonates. These deposits record different morphologies and lithofacies along the discharge path of the rising waters. Bedded travertines were considered the main layers formed during the precipitation of calcium carbonate from saturated water (Vignaroli et al., 2016). According to Brogi et al. (2016), bedded travertine deposits under epigeal conditions from thermal waters. These deposits may have significant slopes and are laminated. In association with the infill of fractures and faults, the so-called banded travertines also appear in the area (Figure 4). They represent the ascent path of hydrothermal fluids to the surface (Brogi et al., 2016). This type of travertine is also usually laminated and crystalline and precipitates under hypogean conditions. These authors also claim that an intimate association exist between banded travertine and seismicity through the mobilization of CO₂-rich waters. In this sense, Uysal et al. (2007 and 2009) argue that banded travertine may reflect tectonic activity in hydrothermal deposits. In Carraclaca, banded travertines filling fractures often cut through the bedded deposits (Figure 4; Figure 5C).

We have identified two main travertine morphotypes in Carraclaca: fissure ridge and cascades.

4.1 Fissure ridge travertine

Fissure ridges are elongated travertine deposits several hundred meters long formed by the connection between multiple aligned

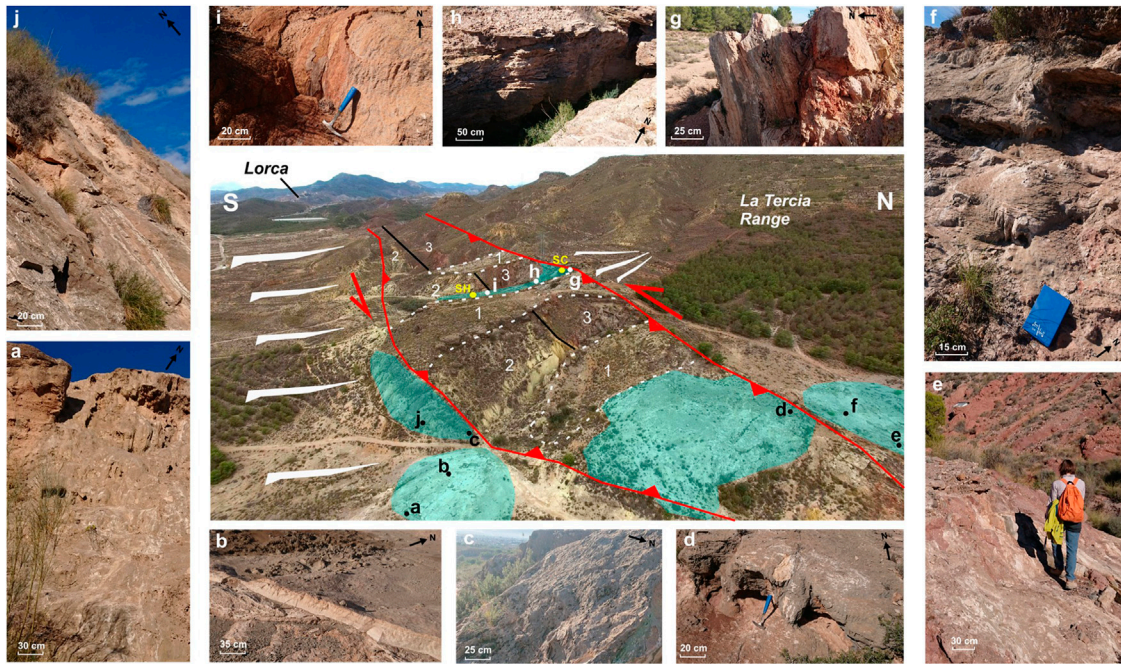


FIGURE 3

The central photo corresponds to an interpretative diagram of the Carraclaca aerial view. The red lines are the faults that limit the tectonic block lifted by two branches of the Alhama de Murcia fault at the base of La Tercia range. The black lines indicate a non-active fault affecting Miocene deposits. Blue coloured areas show travertine deposits. The numbers in the central image refer to the different materials present in the area. (1) Glacis crust. (2) Yellow marls. (3) Red conglomerates and Blue marls. The yellow dots show the position of the water source samples. The letters (A–J) indicate sampling sites. (A) Samples S1 to S4. (B) Sample S6. (C) Sample S5. (D) Samples S7 and S8. (E) Sample S12. (F) Samples S9 to S11. (G) Samples S13 and S14. (H) Samples S15 to S17. (I) Sample S18 (J) Samples S19 and S20.

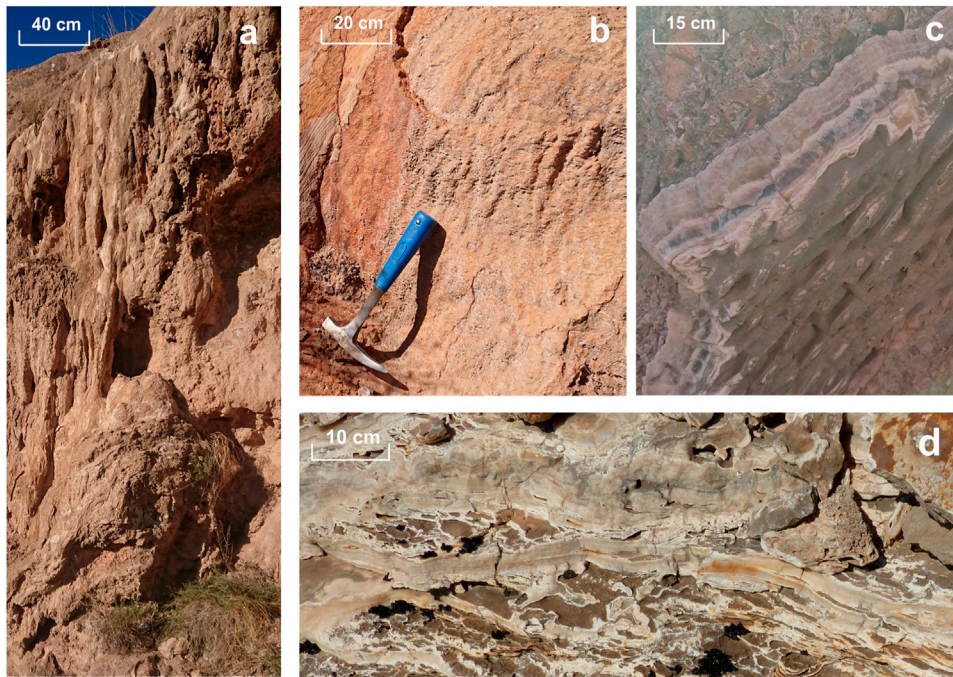


FIGURE 4

Field images of the different outcrops in Carraclaca site. (A) Fluvial scarp where travertine precipitates with cascade-type morphologies. (B) Fault scarp related to the pop-up structure where travertines with cascade morphotypes precipitate. (C) Banded travertine of fracture or fault filling. It shows crystalline crustal lithofacies. (D) Bedded travertine with crystalline crustal lithofacies.

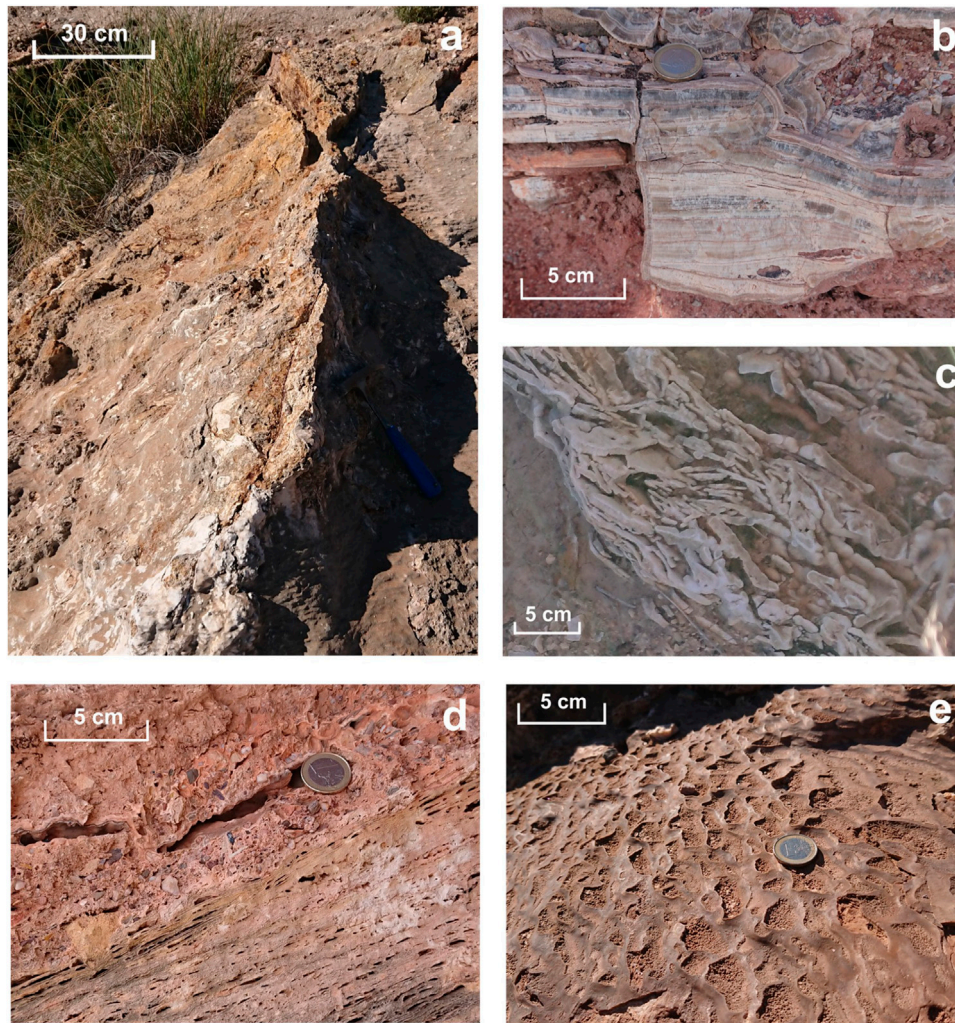


FIGURE 5

Field photographs of the different outcrops in Carraclaca site. (A) Close-up view of a fissure ridges travertine. The long central axis trends in a N-S direction and runs parallel to the secondary fracturing direction. (B) Close-up view of a crystalline crust travertine lithotype. (C) Example of travertine deposit with a Fine-grained lithoclast lithofacies. (D) Bedded travertine with paper-thin raft lithofacies. (E) Close-up view of a minidam sedimentary structure. We can observe the irregular nature of the dams with a rough area inside and polished walls.

sources. They are mound-shaped and have the main opening at the top (Vignaroli et al., 2016). These interconnected mounds gradually increase in height (Zentmyer et al., 2008). According to the Pentecost (2005, chapter 4) classification, fissure ridges are linked to the carbonate waters' thermogenic origin. Hancock et al. (1999) show that this type of morphology appears more frequently in fault stepping zones linked to secondary fractures and not so often in the main fault plane. We can see this in Carraclaca, where the fissure ridge travertine are associated with a conjugate fault system. (Figure 3F). This is 2 m long and 0.5 m height structure with a NNE-SSW trend (Figure 6A). We have found more examples of this travertine morphotype in the area associated with secondary fractures.

4.2 Cascades travertine

The cascade morphotype is typical of areas where the main water channel is accompanied by several smaller currents with reduced

flows. On the areas where the water flows, mosses and hanging plants typical of waterfall deposits develop, sometimes covered with carbonate in the form of speleothems (Arenas-Abad et al., 2010). According to Pentecost (2005, chapter 4), there are two cascading deposits in active sites: erosional and accretionary. The former is common in high discharge currents with vertical falls where erosion is predominant. The latter is more frequent, where the sedimentation rate is higher than the erosion rate. In the study area, we found this type of travertine on the slope of an incised stream located southeast of the Carraclaca pop-up (Figure 3A; Figure 5A) and associated with the northern strand of the structure as well (Figure 3D; Figure 5B). This cascading pattern is fan-shaped and extends perpendicular to the direction of flow. This morphology has been linked to the presence of a fault scarp prior to travertine deposition (Pentecost, 2005).

Associated with these morphologies, at the Carraclaca site, we find sedimentary structures that Pentecost (2005, chapter 4) refers to as Minidams. These small-scale features are typical of thermogenic travertines. Minidams occur in caves and slopes with intermittent

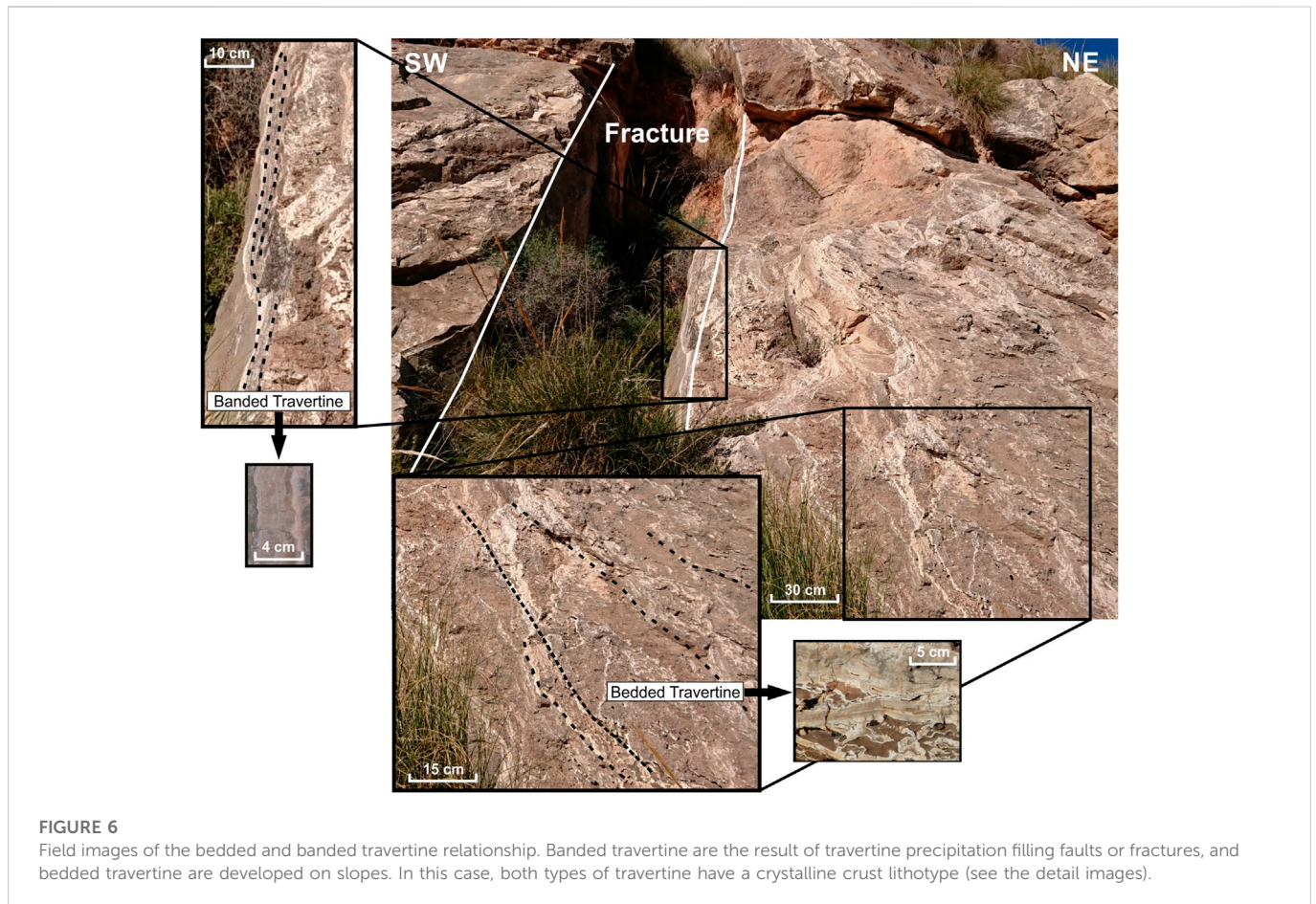


FIGURE 6

Field images of the bedded and banded travertine relationship. Banded travertine are the result of travertine precipitation filling faults or fractures, and bedded travertine are developed on slopes. In this case, both types of travertine have a crystalline crust lithotype (see the detail images).

flow and low water discharge (Pentecost, 2005; Zentmyer et al., 2008). Dams may have asymmetric morphologies with steep or rounded sides and cusps pointing up the slope. The ridge develops preferentially on steeper slopes and tends to be smooth while the spaces between them appear rough (Pentecost, 2005). In the study area, we can identify several points where this type of travertine sedimentary structure appears, independently of the height and inclination of the slope (Figure 6E).

Regarding the texture, granulometry, mineralogy and depositional setting that we can observe in the Carralaca travertine deposits, we have distinguished four travertine lithotypes, as described by Guo and Riding (1998): crystalline crust; fine-grained lithoclast; paper-thin raft; and reed.

4.3 Crystalline crust travertine

This travertine lithotype consists of different layers, ranging from transparent to grey in color, that are probably the result of changes in water chemistry or in the rate of the water flow. The crystalline crust travertines reflect rapid precipitation from fast-flowing waters (Guo and Riding, 1998). That implies a low porosity deposit, although sometimes some porosity may appear between different layers (Gradzinski et al., 2014). It is usual for this type of travertine to have thicker layers as it gets closer to the water source and gets thinner with distance. Thus, changes in the direction and amount of water flow are recorded in accordance with the deposit shape. In Carralaca, this

type of morphology is widespread and results from rainfall on the slope of the travertine mound (Figures 5C, D). We have deposits ranging from 20 cm to 2 m thick, overlapping the Miocene materials. The analysis of microscope and SEM images of crystalline crustal travertine (sample S19) allowed us to recognize the banded growth of elongated fan-shaped calcite crystals (Figure 7). We can also observe the presence of irregular manganese oxide rims separating different fan-shaped growth bands with different crystalline sizes, coloring the sample with different tonalities (Figure 7).

According to Pentecost (2005, chapter 3), the different color and size of the crystalline crust lamination result from a seasonal fluctuation, with thicker dark layers formed in the warm seasons and paler, thinner layers developed during the winter. In the Carralaca site, we can observe this difference in the layers (Figures 6B, Figure 7A), although we have not corroborated that they are due to seasonal changes.

4.4 Fine-grained lithoclast travertine

Lithoclastic travertine is formed by fragments of travertine derived from the rupture of adjacent deposits (Guo and Riding, 1998). According to Gradzinski et al. (2014), this type of travertine originates from the erosion of travertine that previously developed on a slope along with resedimentation stages. It consists of an angular clast of a crystalline crust of a few centimeters in length. These

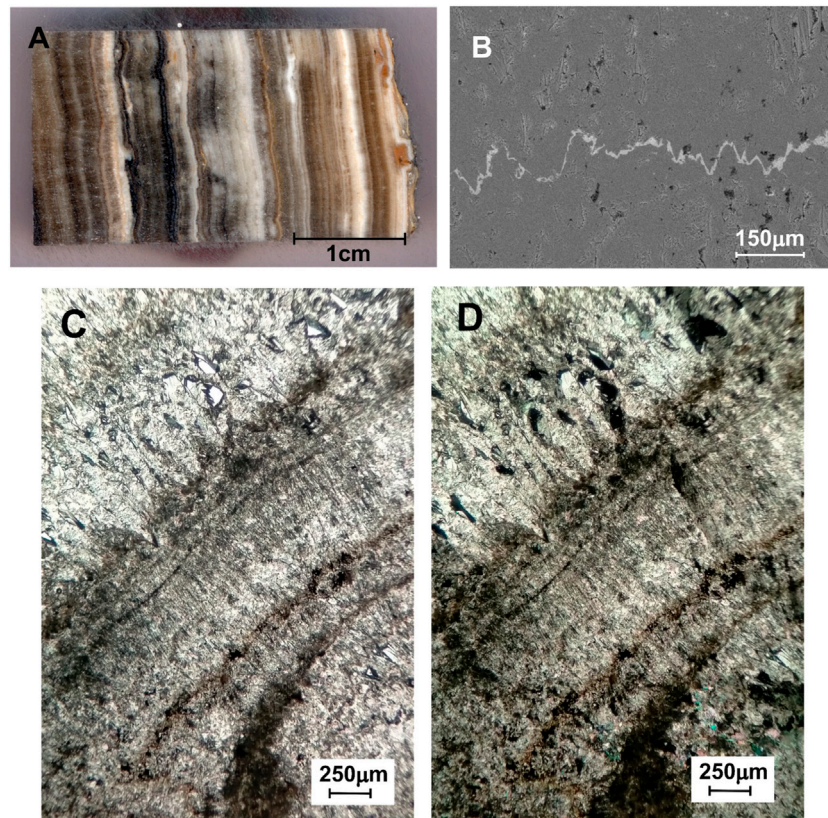


FIGURE 7

Crystalline crust travertine. (A) Polished slab with different coloured crystalline travertine and parallel-banded growth. (B) SEM image showing large calcite crystals and irregular oxides bands (C and D) Thin section with parallel and crossed nicols respectively. Fanshaped crystals alternating with isometric crystals forming crystalline crust travertine.

travertines have a characteristically grain-supported texture and high porosity. In Carraclaca, this type of travertine appears mainly in the base of the southern strand scarp of the pop-up structure (Figure 3C). It is related to the crystalline crust deposits (Figure 6C). SEM and thin section analyses of this lithotype showed non-oriented small size isometric calcite crystals with high porosity and little amounts of presumably iron-manganese oxides randomly distributed within the calcite (Figure 8).

4.5 Paper-thin raft travertine

The paper-thin raft lithotype is described in Guo and Riding (1998) and Gradzinski et al. (2014). This lithotype occurs in depressed areas on the slope of the travertine, which acted as puddles that were a few meters in length. The paper-thin raft travertine consists of thin rafts that grow in the air-water interface with empty spaces between them and accumulates in stagnant waters on the slopes. This environment is widespread near the Carraclaca active spring (Figure 6D), with a particular tendency for ponding water. This lithotype often appears with highly fractured brechoidal facies. Microscope images of sample S20 show tiny calcite crystals with a banded distribution separated by elongated pores (Figures 9C, D). The SEM images show paper-thin raft cores with calcite crystals growing at the edge of the pores (Figure 9B). Gradzinski et al. (2014) have

associated this relationship with the destabilization of raft travertines due to strong wind episodes or seismic ground shaking.

4.6 Reed travertine

According to Guo and Riding (1998), reed travertines are those formed by the precipitation of calcium carbonate around branches or stems. In thermal zones, the high density of plants creates a barrier to water flow. The root systems stabilize the sediment, then the carbonate dissolved in the water is precipitated in contact with the vegetation, crystallizing all the space in between. The roots create cylindrical molds covered by micritic travertine. The vegetation usually disappears and leaves gaps filled with fine-grained material. In the Carraclaca site, we have found these lithofacies associated with cascade-type morphologies in the foothills of travertine deposits (Figure 3A). Microscope and SEM images show high porosity and calcite crystal precipitation in concentric bands around the roots or stems (Figure 10). Sparry cement lining lithoclasts are also visible.

5 Sampling and analytical procedures

We sampled 20 Quaternary travertines throughout the study area for geochemical and mineralogical analysis (Figure 3). Some were

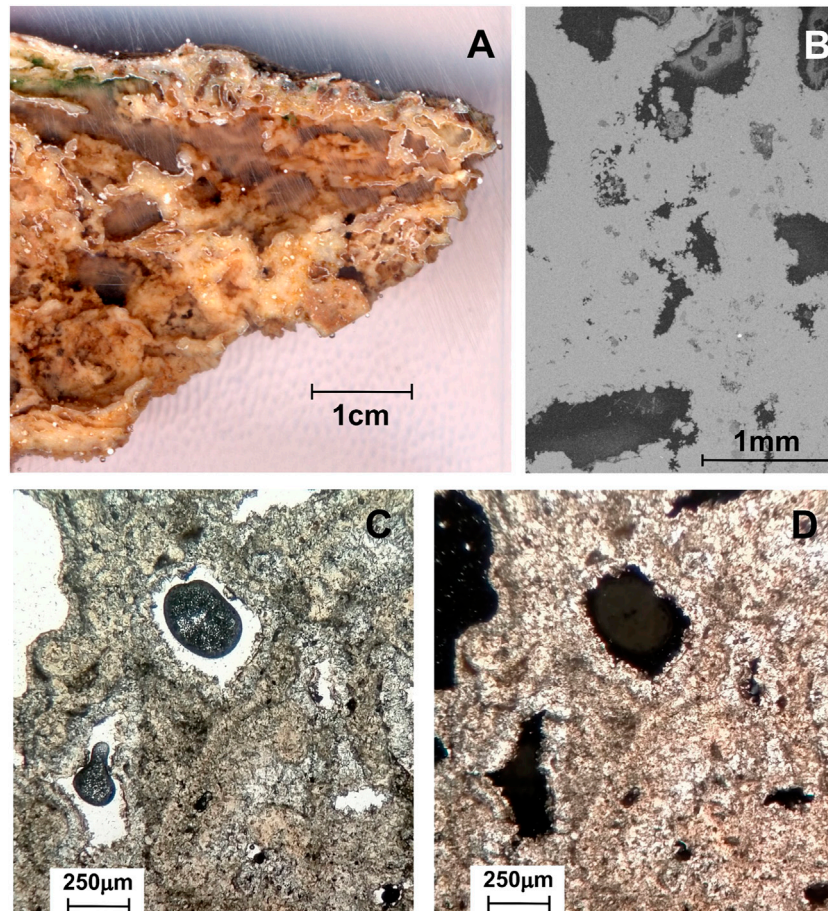


FIGURE 8

Fine-grained lithoclast travertine. (A) Hand specimen photo (B) SEM image showing high porosity and small carbonate crystals (C and D) Microscopic view plane polarized light and crossed nicols respectively. In both, sparry cement lining lithoclasts is visible.

divided into more than one sample due to differences in color, texture, and composition. For sampling, we have considered the lithotypes found in the outcrop and homogeneous spatial distribution. We have also tried to encompass the different structural aspects of the study area. The objective is to have a complete picture of carbonate formation in the Carralaca site and to determine if this could be associated with the AMF seismic activity. For our study, we have also taken samples of different lithologies on which the Carralaca carbonates precipitate and through which water has probably circulated. These rocks are part of the Miocene formations that cover the metamorphic basement rocks uplifted by the fault (see geologic map, Figure 2). They include blue marls and red conglomerates of the Serravallian-Tortonian, Tortonian calcarenites and yellow marls, sandy marls and s.l. marls of the Upper Tortonian-Messinian. To complete the collection from the study area, we took samples from the current water sources (Figure 11) in order to analyze them from a geochemical and mineralogical point of view.

5.1 Water chemistry

Throughout the Carralaca pop-up structure, there are small water upwellings. The most important one is located in the spring inside a

small cave in the northern branch of the structure. That is the principal water catchment point used historically by the now abandoned thermal baths until the first half of the 20th century. For this study, we have analyzed the water from that point (sample CS) and from a smaller spring located about 150 m southeast of the cave (sample HS) (Figure 11). The analysis of the current spring water can give us information about its origin and its relationship with the travertines in the area if any. Water samples were analyzed with a Metrohm dual 861 ionic Chromatograph to determine primary ions. For measuring the anions composition (F, Cl, Br, NO₂, NO₃, PO₄, SO₄), a mixture of carbonate (1.8 mM) and bicarbonate (1.7 mM) was used as eluent. The detection limit is around 0.1 mg/L. To determine the concentration of the major cations (Na, K, Ca, Mg, Sr) chromatographic columns with diluted HNO₃ acid as eluent (1.7 mmol/L) were applied with conductimetric detection. The detection limits are 1 mg/L for Ca and Na and 0.4 mg/L for Mg and K. Alkalinity concentrations were determined by potentiometric titration. Trace elements were measured on the water samples, previously acidulated with suprapure nitric acid with an ICP Spectrometer SPECTRO ARCOS, equipped with a Paschen-Runge optical system and a wave length range between 130 nm and 780 nm. Analytical measurements were performed operating with a modified Lichte Nebulizer to enhance the sensitivity. Detection limits are around 1 ppb, depending on the element.

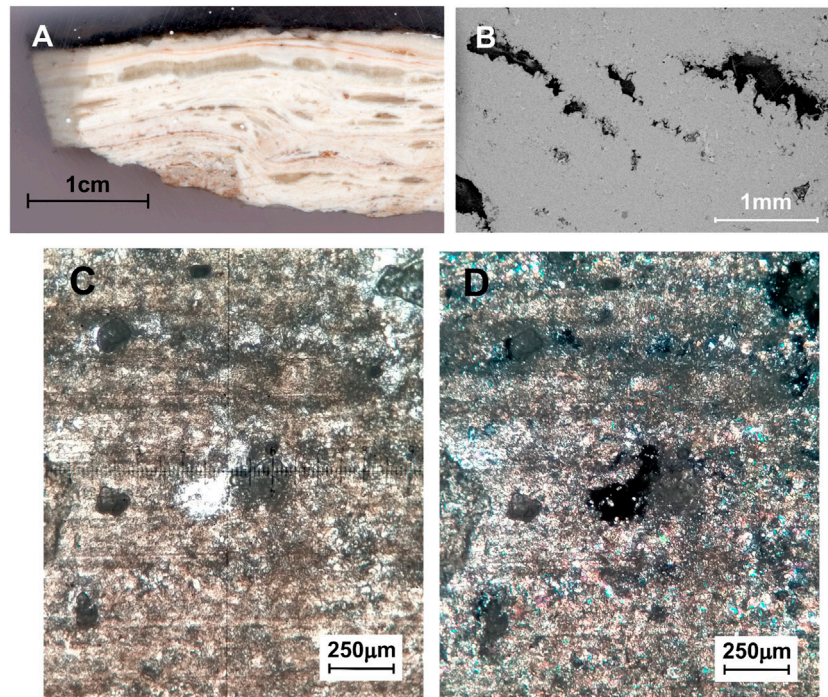


FIGURE 9

Paper-thin raft travertine. (A) Polished slab of paper-thin raft travertine. (B) SEM image showing the growth of calcite crystals in bands separated by pores with crystalline regrowth at their boundaries (C and D) Thin section with parallel and crossed nicols respectively. In the microscopic images, we have micritic cores of paper-thin rafts embedded with scattered calcite crystals.

5.2 Stable isotope analysis

Carbon and oxygen isotopes ($\delta^{13}\text{C}$ and $\delta^{18}\text{O}$) were measured in carbonate samples by Isotope-Ratio Mass Spectrometry (IRMS) VG PRISM IITM. The samples were weighed in exetainer vials, vacuum dried, and H_3PO_4 added. After 18 h at $72^\circ\text{C} \pm 1^\circ\text{C}$, the analysis was performed by continuous flow IRMS, with analytical precision $\pm 0.1\%$. The Carbon and Oxygen data were normalized using international standards (V-PDB) at the Laboratory of Stable Isotope Geochemistry of the Autonomous University of Madrid (UAM).

We have also determined stable isotopes for water samples collected from active springs and geological deposits found in the study area. The aim is to acquire the isotopic signature of these materials in order to discover the relationship between them and the carbonate deposits. Values of $\delta^2\text{H}$ and $\delta^{18}\text{O}$ were determined using CRDS spectroscopy (Cavity Ring-down Spectroscopy, CRDS). Samples were analyzed with a Picarro model L2120 water isotope analyzer coupled with an A0211 high-precision vaporizer. Isotopic deviations δ (‰) are provided related to V-SMOW. Values presented in this paper refer to the isotopic ratios $^{18}\text{O}/^{16}\text{O}$ as well as to $^2\text{H}/\text{H}$, expressed by $\delta^2\text{H}$ ‰ and $\delta^{18}\text{O}$ ‰, allowing a linear fit in a wide range of d values.

5.4 Mineralogical composition

We have analyzed the carbonate samples collected in the field to identify the mineralogical composition using the X-ray diffraction (XRD) technique. The XRD patterns were registered on a Panalytical

X-PERT instrument $\theta/2\theta$ with an X-CELERATOR detector. The mineralogical composition was determined through the Reference Intensity Ratio (RIR) method, which can be considered semi-quantitative. The International Centre of Diffraction Data (ICDD) powder diffraction files (PDF) standards supported in High Score Expert Plus[®] software (version 2.1. b 2005) were used for mineral checking.

We have made an XRD analysis of the 27 travertine samples (Table 3), six sedimentary rocks samples that form the Carralaca pop-up structure, and four samples of materials found in the cave where the main active upwelling appears (Figure 11; Table 4).

5.3 Strontium isotopic ratios and strontium content

In order to identify the relation to potential source rocks of the tufa and travertine deposited carbonates deposited, strontium content and isotopic composition analyses have been carried out on the travertines (Turi, 1986; Pentecost, 2005 (chapter 8); Ozkul et al., 2013; Zentmyer et al., 2008). At Carralaca, we have obtained Sr isotope ratios of both rocks from the different formations involved in the structure and close to the AMF and carbonates, to test the relationship between them. The $^{87}\text{Sr}/^{86}\text{Sr}$ values may indicate that the strontium that appears in a carbonate comes directly from a given rock.

Sr isotopic ratios were measured in a SF-ICP-MS from the Isotope Laboratory at the Centre for Energy, Environmental and Technological Research (CIEMAT) in Madrid, following the methodology described below. A 0.1 g of powdered rock was

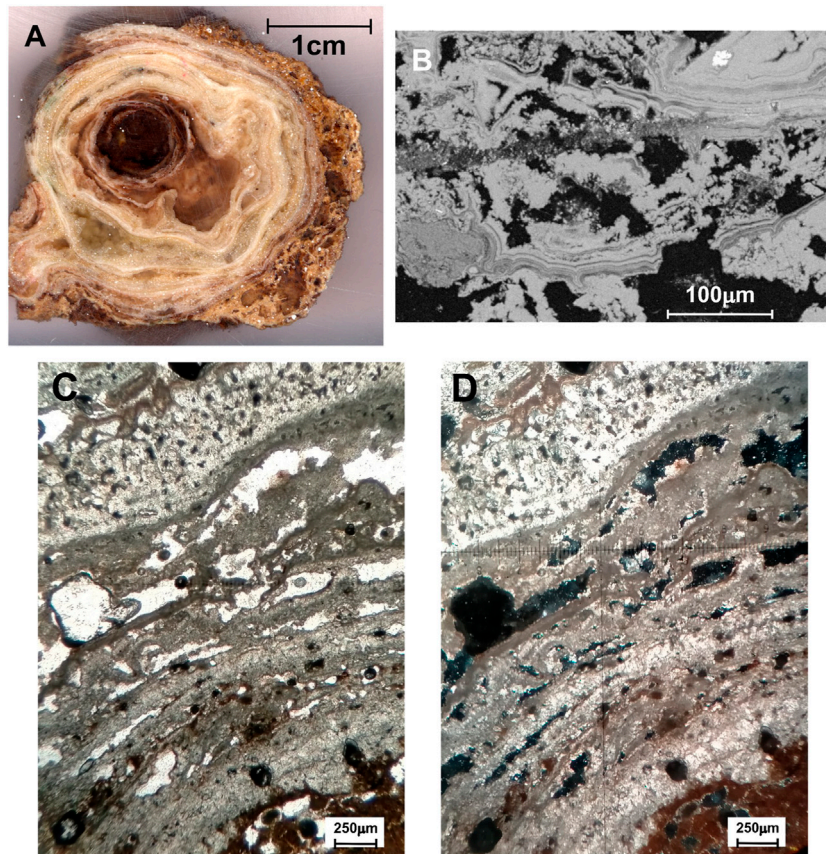


FIGURE 10

Reed travertine. **(A)** Polished slab with the plant cast filled with detritic material in the central zone and concentric carbonate precipitation. **(B)** SEM image showing calcite crystal laminae composed of vertical arborescent structures alternating with micritic levels. We can also observe recrystallization bands crossing the sample **(C and D)** Thin section with parallel and crossed nicols respectively. We observed high porosity and the carbonate growth with concentric disposition alternating with detrital material.

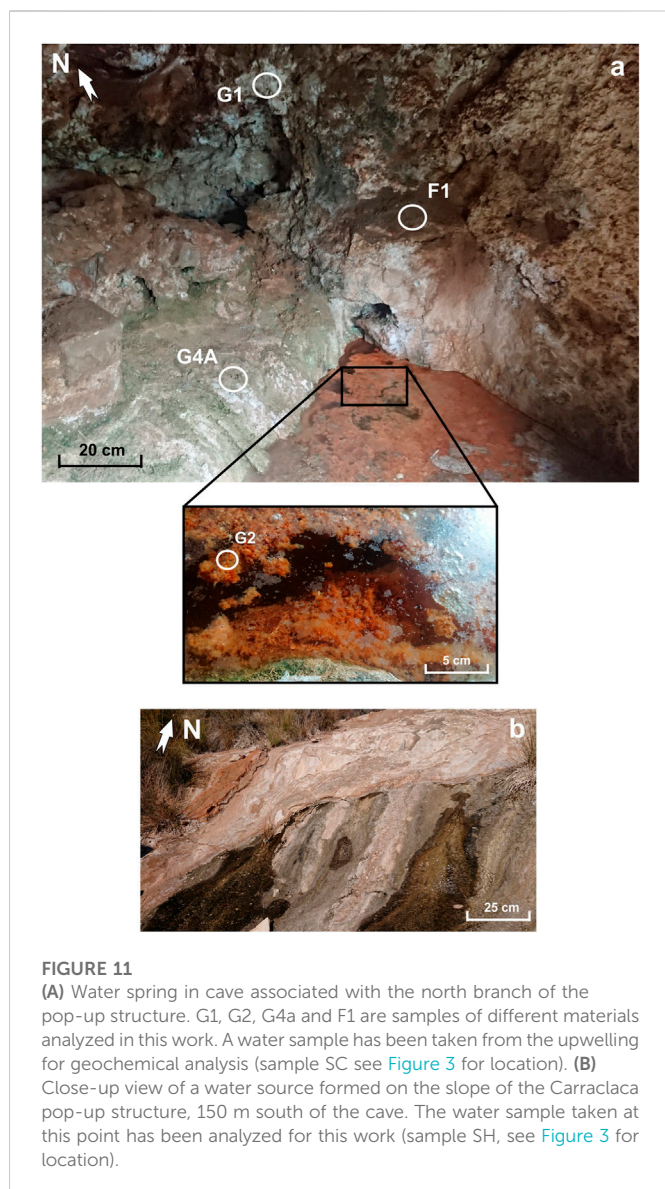
digested overnight in HNO_3 and evaporated to dryness. The residue is dissolved in 2.0 M suprapur nitric acid, and Sr separated of the major cations by conventional ion-exchange chromatography (Sr resin, Eichrom). Sr is recovered from the resin by elution with 2% nitric acid. The samples were measured using the standard bracketing method with an Element two SF-ICP-MS (Thermo Finnigan, Bremen, Germany) equipped with a guard electrode to eliminate secondary discharge in the plasma and to enhance overall sensitivity. The high resolution double focusing (reverse Niers-Johnson geometry) single collector ICP-MS instrument provides flat top peaks in the low resolution mode (m/m 300) which was used for the analysis of ^{85}Rb , ^{87}Sr and ^{86}Sr . A sample introduction kit consisting of a PFA microflow nebulizer, a Peltier-cooled spray cyclonic chamber and a sapphire injector tube (ESI Inc., Omaha, NE, United States) were employed to transport the analytes into the plasma of the ICP-MS. This configuration increases the sensitivity and stability of the conventional sample introduction setup. The solutions were introduced into the plasma using a PFA nebuliser, operating in self-aspiration mode at a flow rate of 50 mL/min. Regarding reagents and standards, all the solutions were prepared with high purity water (18.2 MV cm) from a MilliQ-Element system designed for ultra-trace analysis (Millipore, Milford, MA, United States). Nitric acid (65%, analytical-reagent grade, Scharlab,

Barcelona, Spain) was further purified by sub-boiling distillation (DST-1000 Sub-Boiling Distillation System, Savillex Corporation, United States). Standard calibration solutions were prepared by appropriate dilution of a dissolved amount of NIST 987 certified standard with 2% high-purity nitric acid. Sr isotopic ratios were corrected for mass discrimination using $^{86}\text{Sr}/^{88}\text{Sr}=0.1194$.

6 Results and interpretation

6.1 Water chemistry

According to [Martínez and Moreno \(2005\)](#), the Carralaca active spring had a low flow rate (0.3 L/s) in June 1999. These authors measured an emergence water temperature of 20°C. Today, this situation has not changed substantially. The water pH in the area varies between 7.7 for the CS sample and 7.4 for the HS sample, and the electrical conductivity (EC) is 10,170 and 12,580 $\mu\text{S}/\text{cm}$, respectively ([Table 1](#)). The current rising waters in Carralaca are of the Na-Ca-Cl- SO_4 type. Therefore, besides having a high sodium chloride content, these waters are very hard due to their calcium concentration and have high sulfate concentrations ([Table 1](#)). The lithium content in the water samples is high (12.9 and 9.6 mg/L).



However, this is relatively common in sedimentary environments (Dugamin et al., 2021). In our case, it may be associated with hydrothermalism (Table 1), similar to what occurs in deep tectonic sedimentary basins over crystalline basement in France or Germany (Sanjuan et al., 2022), where hydrothermal water-rock interaction leads to lithium production due to micas dissolution. The $^{87}\text{Sr}/^{86}\text{Sr}$ ratio is also high, suggesting that there are rocks through which water flows before emerging to the surface that provides those isotopic signatures (Table 1; Figure 12). In addition, there is a significant strontium concentration in the samples. The δD and $\delta^{18}\text{O}$ values are in agreement with those obtained by Cerón et al. (1998) for the Guadalestín aquifer waters, which are very close to the study area. The values approach the meteoric line ($\delta^2\text{H}$ SMOW vs. $\delta^{18}\text{O}$ SMOW) of the eastern Mediterranean, indicating a meteoric origin for the water. However, the positive $\delta^{13}\text{C}$ values (ranging between 9.14‰ and 3.73‰) suggest a significant contribution of magmatic CO_2 in the system due to the non-equilibrium fractionation during quick degassing of the dissolved CO_2 gas (Craig, 1961; Filiz, 1984; Ceron et al., 1998; Uysal et al., 2009; Ozkul et al., 2013). Furthermore, the

TABLE 1 Chemistry of the current water springs in Carradaca site.

Sample	CE ($\mu\text{S}/\text{cm}$)	pH	HCO_3 (mg/L)	SO_4 (mg/L)	Ca (mg/L)	Mg (mg/L)	Na (mg/L)	K (mg/L)	Cl (mg/L)	Sr (mg/L)	B (mg/L)	F (mg/L)	Br (mg/L)	Li (mg/L)	$\delta^{13}\text{C}$ VPDB	$\delta^2\text{H}$ SMOW	$\delta^{18}\text{O}$ SMOW	$^{87}\text{Sr}/^{86}\text{Sr}$
Hillshade spring (HS)	12,580	7.4	348	1787	428	106	1583	124	2447	31.9	3.85	1.78	6.19	12.9	3.73	-51.95	-8.10	0.7131
Cave spring (CS)	10,170	7.67	464	1326	460	102	1168	104	1760	24.9	2.84	1.38	4.85	9.6	9.14	-45.75	-9.35	0.7149

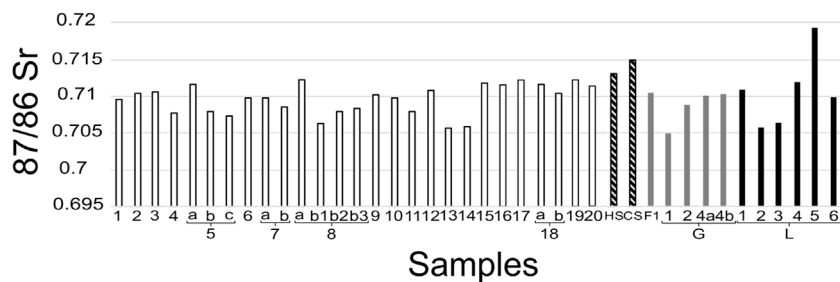


FIGURE 12
Plot of $^{87}\text{Sr}/^{86}\text{Sr}$ ratios for sampled carbonates (white bars), water springs (striped bars), cave materials (grey bars) and Miocene deposits (black bars).

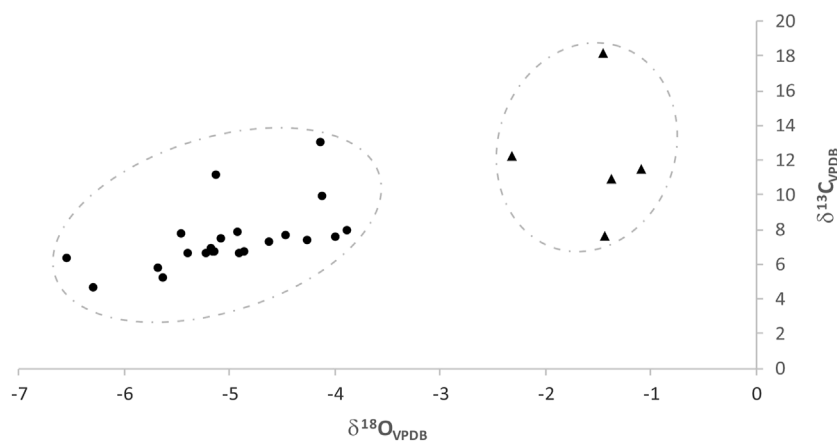


FIGURE 13
 $\delta^{13}\text{C}$ (‰, VPDB) and $\delta^{18}\text{O}$ (‰, VPDB) isotope values diagram obtained for the carbonates samples in Carraclaca site. We can observe a difference in the samples distribution, with those represented by triangles having an enrichment in both isotopes, especially for the oxygen, with respect to those represented by dots.

$\delta^{18}\text{O}$, despite not being a good indicator of the thermal or meteoric origin of the water, rarely appears with values lower than -8.9‰ in meteoric water, according to Pentecost (2005, chapter 8) (Table 1).

6.2 Carbon and oxygen stable isotope composition and paleofluid temperatures

To define the isotopic composition of the Carraclaca travertine, stable carbon ($\delta^{13}\text{C}$) and oxygen ($\delta^{18}\text{O}$) isotope analysis on 27 samples was carried out. Sample locations are shown in Figure 3. All results are reported in Figure 13 and Table 2. The $\delta^{13}\text{C}$ values range from $+4.63$ to $+18.14\text{‰}$ V-PDB, whereas $\delta^{18}\text{O}$ values range from -6.52 to -1.08‰ V-PDB.

$\delta^{13}\text{C}$ values in Carraclaca samples are remarkably positive due to the presence of CO_2 released by magmatic activity in deep areas (Uysal et al., 2009; Kele et al., 2011). Shi et al. (2014) obtain even higher $\delta^{13}\text{C}$ values for travertines formed resulting from precipitation of CO_2 -laden water that rises along the fault systems from deep thermal metamorphism areas. The heavy carbon enrichment could be caused by CO_2 escaping from water in deeper strata. In that case, the light

isotope was enriched first in the gas phase, while the heavy isotope was enriched first in the solid phase (Wang et al., 2007). According to these data, the carbonates in the study area have been formed by precipitation from hydrothermal water. Therefore, the travertines studied have a thermogene origin according to the definition of Pentecost (2005, chapter 2). However, kinetic disequilibrium also results in heavier isotope enrichment that may mislead the issue. In order to rule out this option, the evaporation in the system should be determined based on the δD values. In our case, this is a pending analysis for future work.

The carbon and oxygen stable isotopic signals of Carraclaca samples show two clusters of points (Figure 13). There is a significant statistical difference between the two groups (Supplementary Appendix S1), with one having an enrichment in both isotopes with respect to the other. The difference is mainly in the $\delta^{18}\text{O}$ values, with delta units ranging between -1.08 and -2.31‰ , and -3.87‰ and -6.52‰ V-PDB, respectively. These results indicate a gap between these two types of deposits. This difference may be due to diagenesis processes after deposition or due to the influence of surface water during carbonate precipitation. Martín-García et al. (2002) showed that diagenesis can increase oxygen isotope enrichment

TABLE 2 $\delta^{18}\text{O}$ and $\delta^{13}\text{C}$ isotopic composition and paleotemperatures of Carracalaca site samples.

Sample	Latitude	Longitude	Rock type	$\delta^{13}\text{C}_{\text{VPDB}}$	$\delta^{18}\text{O}_{\text{VPDB}}$	$\delta^{18}\text{O}_{\text{SMOW}}$	T ₁ calculated (°C)	T ₂ calculated (°C)
S1	37°42'18.45"N	1°39'7.78"W	Travitufa	12.18	-2.31	28.53162	7.9 ± 0.5	- 2.4 ± 0.5
S2	37°42'18.47"N	1°39'7.75"W	Travitufa	10.93	-1.37	29.49764	4.1 ± 0.8	- 6 ± 0.8
S3	37°42'18.47"N	1°39'7.80"W	Bedded travertine	7.92	-3.87	26.92116	14.4 ± 0.2	3.6 ± 0.2
S4	37°42'18.39"N	1°39'7.83"W	Travitufa	11.48	-1.08	29.80128	3 ± 0.9	- 7 ± 0.9
S5a	37°42'16.50"N	1°39'11.39"W	Banded travertine	7.80	-4.91	25.8487	18.9 ± 0.7	7.8 ± 0.7
S5b	37°42'16.50"N	1°39'11.39"W	Banded travertine	5.16	-5.62	25.1167	22.1 ± 1	10.7 ± 1
S5c	37°42'16.50"N	1°39'11.39"W	Banded travertine	6.65	-4.84	25.91626	18.6 ± 0.6	7.5 ± 0.6
S6	37°42'16.45"N	1°39'10.43"W	Bedded travertine	7.62	-4.45	26.31736	16.9 ± 0.4	5.9 ± 0.4
S7a	37°42'21.46"N	1°39'8.49"W	Banded travertine	6.61	-5.13	25.62654	19.9 ± 0.8	8.6 ± 0.8
S7b	37°42'21.46"N	1°39'8.49"W	Banded travertine	6.52	-5.20	25.5499	20.2 ± 0.8	8.9 ± 0.8
S8a	37°42'21.46"N	1°39'8.49"W	Bedded travertine	6.57	-4.89	25.87288	18.8 ± 0.6	7.7 ± 0.6
S8b1	37°42'21.46"N	1°39'8.49"W	Bedded travertine	6.56	-5.38	25.36448	21 ± 0.9	9.7 ± 0.9
S8b2	37°42'21.46"N	1°39'8.49"W	Bedded travertine	6.67	-5.15	25.60006	20 ± 0.8	8.7 ± 0.8
S8b3	37°42'21.46"N	1°39'8.49"W	Bedded travertine	6.87	-5.16	25.59168	20 ± 0.8	8.8 ± 0.8
S9	37°42'21.47"N	1°39'9.41"W	Travitufa	7.61	-1.42	29.44575	4.3 ± 0.8	- 5.8 ± 0.8
S10	37°42'21.49"N	1°39'9.30"W	Travitufa	18.14	-1.44	29.42976	4.4 ± 0.8	- 5.7 ± 0.8
S11	37°42'22.87"N	1°39'9.56"W	Bedded travertine	9.89	-4.11	26.67798	15.4 ± 0.3	4.5 ± 0.3
S12	37°42'23.18"N	1°39'5.54"W	Bedded travertine	12.94	-4.11	26.67006	15.4 ± 0.3	4.6 ± 0.3
S13	37°42'18.75"N	1°39'17.20"W	Bedded travertine	6.28	-6.52	24.18458	26.2 ± 1.4	14.5 ± 1.4
S14	37°42'18.75"N	1°39'17.20"W	Bedded travertine	4.63	-6.28	24.43624	25.1 ± 1.3	13.4 ± 1.3
S15	37°42'17.89"N	1°39'20.02"W	Bedded travertine	7.68	-5.43	25.30732	21.2 ± 0.9	9.9 ± 0.9
S16	37°42'17.89"N	1°39'20.02"W	Bedded travertine	7.38	-5.07	25.68435	19.6 ± 0.7	8.4 ± 0.7
S17	37°42'18"N	1°39'19.66"W	Bedded travertine	5.71	-5.66	25.07607	22.2 ± 1	10.8 ± 1
S18a	37°42'16.81"N	1°39'20.15"W	Bedded travertine	7.46	-3.97	26.81594	14.8 ± 0.2	4 ± 0.2
S18b	37°42'16.81"N	1°39'20.15"W	Bedded travertine	7.29	-4.25	26.52746	16 ± 0.4	5.1 ± 0.4
S19	37°42'15.50"N	1°39'11.71"W	Banded travertine	7.20	-4.61	26.16123	17.6 ± 0.5	6.5 ± 0.5
S20	37°42'15.61"N	1°39'11.65"W	Bedded travertine	11.04	-5.11	25.64611	19.8 ± 0.7	8.6 ± 0.7

due to secondary calcite formation and micritization. Looking at the spatial distribution of the samples, we can identify those with the highest oxygen enrichment as the ones farthest away from the water sources. Considering this, along with the morphology of the deposits studied and the analysis of SEM image and thin sections, we are inclined to think that no significant diagenesis processes are present in Carracalaca. Therefore, we argue that the $\delta^{18}\text{O}$ enrichment in some travertine deposits was likely due to precipitation waters of diverse sources and temperature changes during deposition. This process has erased the original isotopic signature of the. We explain the $\delta^{13}\text{C}$ enrichment due to a large CO_2 degassing process before the precipitation of the material.

If we consider the distribution of carbonates samples in the Carracalaca area compared to other materials (Figure 3; Table 2), we can also observe variations in $\delta^{18}\text{O}$ signals. Those deposits found on the old Quaternary glaciais have a much more enriched

oxygen signal than the rest of the travertine, especially compared to those found on yellow and blue Miocene marls. We have made a statistical analysis to corroborate this observation (Supplementary Appendix S1), and we can see a significant statistical difference between these two groups precipitated on Quaternary materials in terms of $\delta^{18}\text{O}$ signal and carbonates precipitated on other materials. The reason for this $\delta^{18}\text{O}$ enrichment may be similar to the one we have provided above to explain the oxygen enrichment with source distance. That means that oxygen enrichment may be due to the influence of meteoric water that flows in a specific area, in this case, through Quaternary materials.

As we have already mentioned, it is possible to calculate the temperatures of the fluids that have generated the carbonates through the oxygen isotopes. This technique, called isotope palaeothermometry, employs equations where the fractionation of equilibrium isotopes during the precipitation of the carbonates is

assumed (Ozkul et al., 2013). We have estimated the formation temperatures of the Carralaca site travertines with the Kele et al. (2015) equation;

$$1000 \ln \alpha = (20 \pm 2) \times 1000/T - (36 \pm 7)$$

where $\alpha = (\delta^{18}\text{O}_{\text{calcite}} + 1000)/(\delta^{18}\text{O}_{\text{water}} + 1000)$ and $103 \ln \alpha - w \approx \delta^{18}\text{O}_{\text{calcite}} - \delta^{18}\text{O}_{\text{water}}$.

The palaeotemperatures are supported by the values of $\delta^{18}\text{O}_{\text{calcite}}$ and $\delta^{18}\text{O}_{\text{water}}$. However, the $\delta^{18}\text{O}_{\text{water}}$ is unknown in the case of fossil travertine deposits, so it must be inferred. That can involve deviations up to 9°C, according to Kele et al. (2011). We have used available regional and local data on water composition to determine the parent waters. These have implied two different $\delta^{18}\text{O}$ values for parent water. One is the present-day $\delta^{18}\text{O}$ value of the Lorca wells in the Totana aquifer (−6.63‰ Vienna standard mean ocean water [VSMOW]), which is characterized by a constant temperature of 23.35°C (Rodrigo-Navarro et al., 2013). The second is the $\delta^{18}\text{O}$ value obtained from the cave water sample (CS sample) (−9.35‰ V-SMOW).

In the first scenario, it is assumed that the composition of the oxygen isotopes of the travertine parental water is close to that of the currently active Lorca spring. Calculated paleotemperatures posted in Table 2_T1 range between 3°C and 26.2°C. In the second scenario, we assume a parent water $\delta^{18}\text{O}$ value similar to that of the Carralaca active spring. Hence, calculated paleotemperatures range between a −7°C and 14.5°C (Table 2_T2), which is about 10°C less on average than the previous range. These temperatures are unrealistic and lead us to think that the current water chemistry at Carralaca must differ from that which led to the travertine deposits in the area. In addition, it must be noted that groundwater chemistry is unknown and different compositional effects involving isotopic fractionation could occur (Zhou and Zheng, 2006).

In any case, paleotemperature values indicate an oxygen signature that signifies cool precipitation temperatures, possibly related to the mixing between thermal upwelling and meteoric water. It is also possible that, as in some Turkish travertines (Kele et al., 2011; Ozkul et al., 2013), the loss of ^{16}O from water due to evaporation can indirectly increase the travertine's $\delta^{18}\text{O}$ values, significantly lowering temperatures.

6.3 Mineralogy

Calcite is the most common mineral in the carbonates of the study zone, as we could verify with XRD analyses of the 27 travertine samples (Table 3). It is in fact low-Mg magnesian calcite, with 2% mol MgCO_3 in most of the samples, as was established as follows (Supplementary Figure S1). Low-Mg calcite showed a d 104 reflection at 3.04–3.02 Å (Zhang et al., 2010; Fahad and Saeed, 2018; Stanienda Pilecki, 2018). The mol% of MgCO_3 has been calculated using the data of Fahad and Saeed (2018) since low-Mg calcite in relation to the Mg content of calcite has been correlated to an increase in temperature (Burton and Walter, 1987). Aragonite is also present in some samples but very sparingly (up to 8%), and it is mainly related to those with a higher oxygen and carbon enrichment. Some of these samples contain detrital minerals (quartz, muscovite, or chlorite) and gypsum in variable amounts (Table 3), although most contain only calcite.

XRD analyses from the substrate rock samples (L1 to L6 in Table 4) show high variability in composition. Although they all have calcite, quartz, and muscovite, the percentages of each of

these minerals are very different for each sample. The rocks show higher amount of detritic minerals than the carbonates analyzed above. That is reasonable if we consider that they are mainly detritic sedimentary rocks. Sample L6 consists mainly of gypsum and contains 10% of muscovite and 6% of dolomite (Table 4). Sample L1 and L5 have a significant amount of clinoclone-like chlorite. The difference is that while the L1 (blue marls) has a large amount of quartz (65%), the L5 (red conglomerates) has a similar concentration of quartz and calcite, which is around 25% (Table 4).

The x-ray analyses carried out on the materials extracted from the cave indicate materials of very different compositions (Table 4). Sample F1 is entirely goethite. Sample G1 is composed mainly of halite (87%). The colloid that appears floating on the surface of the water source (sample G2) is mainly a calcite aggregate with a limited amount of gypsum. Finally, the sample G4A corresponds to a material that covers the cave walls. It has an intermediate composition between halite and goethite, with a significant percentage (10%–15%) of cristobalite and glauberite (Table 4). These deposits are characteristic salt efflorescences related to capillarity in which salts with different composition, related to the chemistry of circulating solutions, precipitates when water evaporates in open contact to atmosphere at the cave walls.

There are numerous minerals in the study area forming the analyzed materials. However, we can determine that the deposits of Carralaca are predominantly formed by calcite, precipitated in moderate to high saline aqueous media. Iron oxy-hydroxide minerals deposits form small bands intercalated in crystalline calcite travertine. Their origin could be related to the sporadic circulation of reduced Iron (II) rich fluids coming from Fe (II) reservoirs (as blue marls), which precipitated in contact with an oxidizing meteoric environment. Thus, indicating the alternance of upwelling fluids that flow through different materials at different depths.

6.4 Strontium isotopic ratios and strontium content

As we have previously indicated, when a fluid passes through a rock at depth, it is marked by an isotopic ratio of $^{87}\text{Sr}/^{86}\text{Sr}$, reflecting the geochemistry of that rock. Once the fluid reaches the surface and precipitates in the form of travertine, it is imprinted with the same isotopic strontium composition as the water from which it came. According to Pentecost (2005), values between 0.708 and 0.7125 for strontium isotope ratios are related to limestones, evaporites, and marl. In addition, $^{87}\text{Sr}/^{86}\text{Sr}$ values in the range of 0.72–0.78 seem to be related to metamorphic rocks that lead the travertine (Spötl et al., 2002).

$^{87}\text{Sr}/^{86}\text{Sr}$ ratios for the Carralaca samples show very high variability, both in the carbonate materials and in others (Table 5; Figure 12). Values for travertines range from 0.7056 to 0.7123, with a mean of around 0.7093. According to Pentecost (2005), those values could suggest a sedimentary source (evaporates, limestones, or marls). The $^{87}\text{Sr}/^{86}\text{Sr}$ values calculated for the Carralaca sedimentary rocks are also diverse, ranging from 0.7057 to 0.7192 (samples L1 to L6 in Table 5; Figure 12). This diversity in the sediments signature may explain, in turn, the wide range of data shown by the carbonates. The strontium isotopic ratios in Carralaca's travertines are showing that the spring water passed through the radiogenic basement in its rise to

TABLE 3 Mineralogical compositions of the Carraclaca site samples based on XRD analyses. ++: >10%. +: 5%–10%. Id: identified.

Sample	Rock type	Basement deposit	% calcite	Mg-calcite	% Quartz low	% aragonite	% Moscovite	% gypsum	% Chlorite
S1	Travitufa	Quaternary	95	id	1	3	1	<1	<1
S2	Travitufa	Quaternary	90	id	6	1	1	1	1
S3	Bedded travertine	Quaternary	75	++	24	<1	<1	<1	<1
S4	Travitufa	Quaternary	83	+	5	8	1	<1	2
S5a	Banded travertine	Yellow Marls	98	id	<1	<1	<1	<1	<1
S5b	Banded travertine	Yellow Marls	94	++	6	<1	<1	<1	<1
S5c	Banded travertine	Yellow Marls	99	++	<1	<1	<1	<1	<1
S6	Bedded travertine	Quaternary	99	++	<1	<1	<1	<1	<1
S7a	Banded travertine	Conglomerates	98	id	<1	<1	<1	<1	<1
S7b	Banded travertine	Conglomerates	99	++	<1	<1	<1	<1	<1
S8a	Bedded travertine	Conglomerates	99	+	<1	<1	<1	<1	<1
S8b1	Bedded travertine	Conglomerates	99	+	<1	<1	1	<1	<1
S8b2	Bedded travertine	Conglomerates	99	+	<1	<1	<1	<1	<1
S8b3	Bedded travertine	Conglomerates	99	+	<1	<1	<1	<1	<1
S9	Travitufa	Conglomerates	98	++	1	<1	<1	<1	<1
S10	Travitufa	Conglomerates	69	id	26	2	<1	2	<1
S11	Bedded travertine	Conglomerates	98	++	1	1	<1	<1	<1
S12	Bedded travertine	Conglomerates	85	++	7	7	1	<1	<1
S13	Bedded travertine	Blue Marl	88	+	2	<1	1	<1	<1
S14	Bedded travertine	Blue Marl	99	++	<1	<1	<1	<1	<1
S15	Bedded travertine	Blue Marl	86	id	14	<1	<1	<1	<1
S16	Bedded travertine	Blue Marl	99	+	<1	<1	<1	1	<1
S17	Bedded travertine	Blue Marl	96	+	3	<1	<1	<1	<1
S18a	Bedded travertine	Blue Marl	99	+	<1	<1	<1	<1	<1
S18b	Bedded travertine	Blue Marl	99	++	<1	<1	<1	<1	<1
S19	Banded travertine	Yellow Marls	98	id	<1	<1	<1	<1	<1
S20	Bedded travertine	Yellow Marls	99	+	<1	<1	<1	<1	<1

TABLE 4 Mineralogical compositions of the cave deposits and Miocene sediments in Carraclaca site based on XRD analyses.

Sample	Facies	% calcite	% Quartz low	% Muscovite	% Gypsum	% Hematite	% Goethite	% Halite	% Glauberite	% Cristobalite	% Clinoclhoride	% Paragonite	% Chlorite	% Ankerite	% Dolomite	% Coelestine
F1	Cave wall covering	<1	<1	<1	<1	<1	100	<1	<1	<1	<1	<1	<1	<1	<1	<1
L1	Blue marls	2	64	11	<1	2	<1	<1	<1	<1	17	5	<1	<1	<1	<1
L2	Calcarenite	45	40	3	<1	<1	<1	<1	<1	<1	<1	8	4	<1	<1	<1
L3	Yellow marls	63	22	5	2	<1	<1	<1	<1	<1	4	<1	<1	4	<1	<1
L4	Marls s.l	41	29	5	<1	<1	<1	12	<1	<1	7	<1	<1	<1	3	<1
L5	Red conglomerate	27	25	7	3	2	<1	<1	<1	<1	16	2	<1	4	9	<1
L6	Sandy marls	4	3	10	75	<1	<1	<1	<1	<1	2	<1	<1	<1	6	<1
G1	Cave wall covering	<1	5	<1	87	<1	<1	1	7	<1	<1	<1	<1	<1	<1	<1
G2	Colloid	81	6	1	12	<1	<1	<1	<1	<1	<1	<1	<1	<1	<1	<1
G4A	Cave wall covering	<1	2	<1	<1	<1	47	21	15	10	<1	<1	<1	<1	<1	4

TABLE 5 $^{87}\text{Sr}/^{86}\text{Sr}$ ratios and Sr content of the carbonates, and $^{87}\text{Sr}/^{86}\text{Sr}$ ratios of the cave deposits and Miocene sediments in Carraclaca site.

Sample	Facies	$^{87}/^{86}$ Sr	Sr (mg/100 g)
S1	Travitufa	0.70958	814,4
S2	Travitufa	0.71029	774,8
S3	Bedded travertine	0.71049	530,7
S4	Travitufa	0.70766	947,7
S5a	Banded travertine	0.71155	431,9
S5b	Banded travertine	0.70782	270,6
S5c	Banded travertine	0.70722	187,7
S6	Bedded travertine	0.70972	482,4
S7a	Banded travertine	0.70972	301,2
S7b	Banded travertine	0.7086	354,2
S8a	Bedded travertine	0.71225	336,7
S8b1	Bedded travertine	0.70634	139,2
S8b2	Bedded travertine	0.70793	202,8
S8b3	Bedded travertine	0.7083	141,3
S9	Travitufa	0.71015	356,0
S10	Travitufa	0.7098	915,8
S11	Bedded travertine	0.70788	391,5
S12	Bedded travertine	0.7108	717,5
S13	Bedded travertine	0.70557	152,6
S14	Bedded travertine	0.70588	132,8
S15	Bedded travertine	0.71177	450,8
S16	Bedded travertine	0.71155	508,0
S17	Bedded travertine	0.71232	293,7
S18a	Bedded travertine	0.71157	196,7
S18b	Bedded travertine	0.71031	252,1
S19	Banded travertine	0.712115	206,3
S20	Bedded travertine	0.71132	251,9
F1	Cave wall covering	0,71051	—
L1	Blue marls	0,71097	—
L2	Calcarenite	0,70569	—
L3	Yellow marls	0,70637	—
L4	Marls s.l	0,71188	—
L5	Red conglomerate	0,71923	—
L6	Sandy marls	0,70978	—
G1	Cave wall covering	0,70494	—
G2	Colloid	0,70891	—
G4A	Cave wall covering	0,71016	—

the surface. Considering this, we can suggest that the travertines studied come from water that has followed different paths in their ascent to the surface. Thus, travertines with lower strontium isotope

ratios may be derived from springs-fed water that dissolved the calcarenite and the yellow marls (samples L2 and L3). While carbonates with high $^{87}\text{Sr}/^{86}\text{Sr}$ values may be more related to ascent paths through the red conglomerates or the marls s.l. (samples L4 and L5). The high values of the strontium isotopic ratios that are present in the active water springs (Table 1; Figure 12) are noteworthy. We explain this by considering that the current fluid ascent channel passes through the red conglomerates (sample L5) or through metasedimentary rock in the basement.

Data variability suggests the need for a more detailed study to determine the source of the strontium signal in Carraclaca carbonates.

Regarding the strontium content (Table 5), there is a statistically significant relationship between Sr and $\delta^{13}\text{C}$ VPDB at the 95% confidence level (p -value <0.05) in the Carraclaca carbonates (Supplementary Appendix S1; Supplementary Figure S2). We can observe that the highest strontium concentrations occur in the oxygen- and carbon-enriched samples (up to 947.7 mg/kg). The high strontium concentrations in these travertines may be related to the interaction between the groundwater from which they are derived, and the Late Tortonian-Messinian evaporites (Minissale et al., 2002). Malone and Baker (1999) determined a relationship of increasing Sr/Ca ratios in calcite related to the rise of temperature from 40°C to 200°C, specifically well-established when dolomite dissolved to form calcite. This observation agrees with the relationship of $\delta^{13}\text{C}$ enrichment with the temperature of the fluids conditioning calcite formation in the Carraclaca carbonates. The same authors also observed an increase in the Mg mol ratio of calcite with Sr. Although it is not shown in the paper, Mg contents in Carraclaca calcites are also significantly correlated ($r = 0.53$; p -value <0.05).

7 Discussion

7.1 Tectonic control of the site

Many studies have been carried out on the recent activity of the AMF with the objective of characterising its sismogenic behaviour, slip rate, major earthquake recurrence time, maximum magnitude, etc. (e.g. Masana et al., 2004; Ortuño et al., 2012; Martí et al., 2016; Ferrater et al., 2017; Herrero-Barbero et al., 2017; Martínez-Díaz et al., 2018; Rodríguez-Escudero et al., 2020; Gomez-Novell, 2021). Our paper aims to study the relationship between the AMF seismic cycle and the time and space morphology and geochemistry changes of Carraclaca carbonates to obtain additional paleoseismic information.

The great majority of travertines associated with active faults are related to normal faults or extensional sectors of strike-slip and oblique-slip faults (Zentmyer et al., 2008; Ascione et al., 2013; Ozkul et al., 2013; Capezzuoli et al., 2014; Brogi et al., 2016; Vignaroli et al., 2016). In these cases, the extension produced by the fault activity favours permeability, creating pathways along which the calcium and carbonate-loaded fluids can rise to the surface and precipitate, forming travertines and tufas. There are far fewer studies where travertine is related to the activity of strike-slip faults (DeFilippis et al., 2013; Temiz et al., 2013; Colak et al., 2015). All these later studies have in common that the travertines appear associated with the transtensive zones of the faults. That is reasonable considering that fluids must have enough space to rise to the surface. There are some examples of mantle fluids escaping to

the atmosphere in compressional geological settings (Caracausi and Sulli, 2019), but these are less frequent scenarios. Therefore, the structure of the fault zone is an important factor.

As we have already mentioned, the AMF is a sinistral strike-slip fault with a reverse component that generates the kilometer-scale asymmetric fold that forms the Sierra de la Tercia Range (Figure 1) (Martinez-Díaz, 2002). That induces a transpressional shear of the subvertical fold limb (Alonso-Henar et al., 2018).

Therefore, the study area represents a rare case of a travertine system in a transpressive area. The compressional component of the strain regime, active in the Lorca-Totana section of the AMF (corroborated by the focal mechanism of the Mw 5.2, 2011 Lorca earthquake (Figure 1B)), does not promote vertical permeability. Furthermore, according to the classic fault-valve model of Sibson (1990), faults act as impermeable seals, especially those active, despite being oriented unfavorably for frictional reactivation. That is true except for the time immediately following the seismic rupture when they become highly permeable pathways for fluids. According to Sibson (2004), extreme valving action involving significant fluid volumes is associated with high dipping (>60°) reverse faults that are strongly misoriented. Therefore, we consider that seismic activity in the AMF could open the fracturing system favoring the ascent of deep fluids that create the travertines, despite the cinematic context.

7.2 Hydrothermal circulation and travertine formation

As we mention above, the Carralaca travertines arise in connection with the pop-up structure generated by the activity of the northern branch of the Lorca-Totana section of the AMF. The faults here have a transpressive component that creates a double monocline affecting recent deposits. The spatial relationship between recently active faults and the distribution of travertine deposits in our study area suggests that the deep CO₂-laden water that rises to the surface moves along these active structures. The complexity of the fault zone structure allows the existence of several thermal springs at different positions (Figure 2). In Carralaca, we have found two different depositional morphologies (fissure ridges and cascades) and one sedimentary structure (minidams) along the fault trace. Among these morphologies, the Carralaca travertines occur in four lithotypes: crystalline crust; fine-grained lithoclast; paper-thin raft; and reed. The distribution of the different travertine samples in the study area shows that those with reed and fine-grained lithoclast lithotypes are located farther away from the water sources. These are materials characterized by smaller calcite crystal size and higher porosity (Figures 8, 10). In contrast, the travertines closest to the springs are crystalline crust and paper-thin raft travertines, with low porosity, laminar structure, and higher crystalline growth (Figures 7, 9). Taking into account the textural differences within our samples, we could discriminate in Carralaca between travertines and tufas in the sense that Rodríguez-Berriguete and Alonso-Zarza (2019) and Teboul et al. (2016) do. Thus, travertines would be the crystalline and less porous textured deposits, related to abiotic processes and characterized by high depositional rates, while tufas would have a micritic aspect, related to biotic processes with abundant plant-like facies, highly porous, and typified by low depositional rates.

A possible hypothesis to explain the Carralaca travertine features would be as follows: water rises along faults transporting carbonates in

solution to the surface. Once the water sheet emerges through different fissures, it flows down the slope causing the travertine precipitation in the crystalline crustal and paper-thin raft lithotypes in the areas closest to the upwellings. Further away, associated with cascade-type morphologies, carbonate precipitation occurs in reed lithotypes, with more interaction with vegetation.

As a second stage, rockfall events due to earthquakes would produce fine-grained lithoclasts. The shaking would cause the pre-existing travertine deposits to break up and accumulate in some slope areas. The loose clasts would quickly lithify due to the flow of water promoted by the earthquake, generating fine-grained lithoclast travertines. However, there may be alternative explanations for these travertine formations, such as aseismic landslides promoted by large floods.

To determine the evolution and relationship of the Carralaca travertines to fault activity, the age of each type of deposit would need to be known. The minimum age of tectonic activity on a fault can be established by its relationship to travertine deposits. In addition, it would be possible approximate paleoseismic events of the AMF. For this purpose, the banded travertine will be of great interest, since it is closely related to the seismic activity in the area, possibly resulting from the ascent of fluids along fractures caused by earthquakes. The episodic thin Mn-oxide rims separate different crystal size aggregates of the calcite rims and can be also representative of different events of water rise and carbonate deposition related to seismic activity. It will be important to make in the future detailed studies of isotopic signatures and to measure subtle changes, for instance in the Sr and Mg contents in calcite, within the consecutive carbonate rims. If signature gradients are detected, this will aid to confirm the existence of dynamic water mixing regimes and also deep evaporation processes related to hydrothermal origin fluids, affecting the ¹³C enrichment in the surface precipitated carbonates.

Although calcite is the main mineral found in all Carralaca samples, generally with low Mg contents, aragonite is also present. The results of our carbon and oxygen isotope analyses support at least in part the idea that the Carralaca deposits have a deep-derived carbon source. However, the study reveals more positive values of δ¹³C than usual for thermogene travertines, probably due to CO₂ degassing downstream. In addition, values indicate formation temperatures around 20°C. That temperature is consistent with non-thermal water precipitation or water-cooled in its flow to the surface. That is the case in current spring water analyses, where δD and δ¹⁸O values indicate a meteoric origin and the δ¹³C values indicate a contribution of magmatic CO₂. However, it is especially evident in the tufa deposits found in the study area. These deposits, in spite of presenting very positive δ¹³C signatures (which would indicate a hydrothermal origin), also have highly enriched δ¹⁸O values, indicating low precipitation temperatures. Therefore, they should be considered thermogenic travertines from a geochemical standpoint. However, the properties and dispositions of the facies are better suited to the term tufa (Camuera et al., 2014; De Pinho et al., 2015). Accordingly, this group of tufas is characterized by an isotopic signal typical of deep-water precipitation at ambient temperature. According to Cappezuoli et al. (2014), these deposits appear near geothermal regions associated with active faults. These authors suggested the term 'travitufa' for those ambient temperature deposits characterized by deep-circulating hydrochemical signatures to differentiate them from regular tufas. Our data totally agree with the approach of these authors for the tufas found at the Carralaca site since they are

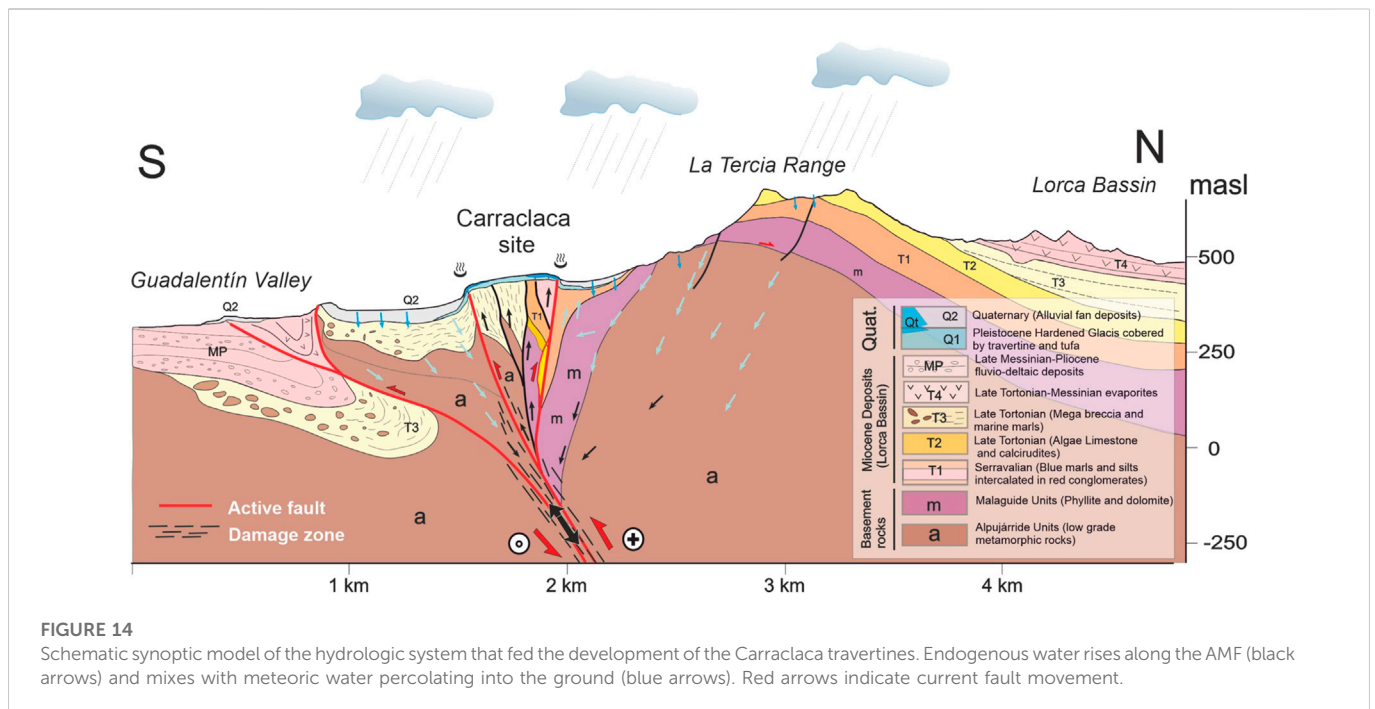


FIGURE 14

Schematic synoptic model of the hydrologic system that fed the development of the Carralaca travertines. Endogenous water rises along the AMF (black arrows) and mixes with meteoric water percolating into the ground (blue arrows). Red arrows indicate current fault movement.

deposited, in most cases, tens to hundreds of meters from the water sources.

7.3 Synoptic preliminary model

Based on the tectonic setting and the carbon and oxygen isotope results, we have created a model in order to explain the travertine and tufa formation in Carralaca (Figure 14). In several works (Crossey et al., 2006; Zentmyer et al., 2008; Gradzinski et al., 2014), hydrological models are presented that explain travertine deposits as the result of the mixture of meteoric water circulating at a shallow depth with deep endogenous water, in variable proportions. In these models, even a minor contribution from deep water can strongly condition the geochemistry of the water, substantially modifying its isotopic signature (Newell et al., 2005; Crossey et al., 2006; Zentmyer et al., 2008). In our model, meteoric water leaked through the Miocene Lorca basin deposits. These materials are folded and tilted by the AMF, favoring subvertical pathways and guiding the water flow into the deeper part of the fault zone. The model assumes that some of the fluid must interact with the radiogenic rocks beneath the Miocene sequence. Therefore, the Carralaca travertines can be interpreted to have formed by degassing and precipitation of CO_2 -enriched hydrothermal fluids rising to the surface through active faults and mixing with cooler surface meteoric waters.

Considering the results of the $^{87}\text{Sr}/^{86}\text{Sr}$ ratios analysis, we can deduce that the fluid ascent paths produced by the fault are complex, undoubtedly induced by the structural complexity of the fault zone. It is possible that after each tectonic episode (earthquake rupture), new fault paths open in the area, being sealed afterward, leaving a characteristic strontium isotopic imprint in the precipitated travertine.

The AMF has been a high-angle transpressive structure since the late Miocene (Martinez-Diaz, 2002; Alonso-Henar et al., 2018). In this tectonic context (mainly in high-angle compressional faults), the

sealing of permeability over time is more efficient than in extensional faults (Sibson 2004). Therefore, travertine systems in a compressional or transpressive regime are not frequent.

Large earthquakes with shallow rupture along this fault section would generate large permeability changes (Sibson, 1996; Curewitz and Karson, 1997; Giwelli et al., 2016), but are quite rare. In contrast, climatic and seasonal variations in an arid region, such as the study area, create smaller effects. The latter are much more common and may act on larger spatial scales. That makes Carralaca travertines particularly interesting for analyzing the relationship between travertine characteristics and tectonically induced permeability variations. That would lead us to use these materials as “paleoseismometers” capable of recording large earthquakes with surface rupture, which complements classical paleoseismology. Therefore, a detailed dating of the observed sedimentation episodes would be a helpful tool to characterize the seismic cycle of the AMF and quantify the recurrence of large earthquakes on this fault.

8 Conclusion

The Plio-Quaternary carbonate deposits of the Carralaca site reflect the interaction between hydrothermalism, active tectonics, and meteoric water in a region characterized by moderate seismicity. In the study area, travertine precipitation occurred along the faults that form a pop-up structure related to the transpressive nature of the AMF, which accommodates most of the deformation in the single shear component in the Lorca-Totana section. The travertine deposits studied have had different precipitation environments, resulting in two morphotypes; fissure ridge travertine and cascades, as well as four lithotypes; crystalline crust travertine, fine-grained travertine, paper-thin rafts travertine, and reed travertine. Differences in the activity and structure of the fault zone are responsible for the diverse types of morphologies and lithofacies found in Carralaca.

Current spring water found in the study area has deep flow paths based on its carbon, oxygen, and deuterium signatures, consistent with the isotopic analysis of the Carralaca travertines and tufas. In order to explain the origin of the fluids that give rise to the carbonates, we have proposed a model in which meteoric water mixes deeply with endogenous CO₂-rich fluids. The resulting flow uses the structure of the Alhama de Murcia Fault as a pathway to the surface. The ⁸⁷Sr/⁸⁶Sr ratios obtained for the travertine show the necessary interaction between the subsurface water, the Miocene basin sediments, and the radiogenic rocks of the basements, such as those of the Alpujarride units.

The transpressive regime of the AMF is not favorable for the development of travertine deposits since this fault has a higher permeability seal. Even so, we have established that the Carralaca deposits are related to fault activity. That makes Carralaca travertines especially interesting for analyzing the relationship between travertine characteristics and transient permeability variations that are tectonically induced.

The association of travertine with the activity of a main tectonic structure within the eastern Betic rangeis of great interest for the seismic hazard assessment and justifies further exploration of deposits through the study of its age and the paleoseismic record.

Data availability statement

The original contributions presented in the study are included in the article/[Supplementary Material](#), further inquiries can be directed to the corresponding author.

Author contributions

CC and JM conceived the study, carried out the mapping and took the field samples. JR and AG performed the chemical analysis. CC

References

- Alonso-Henar, J., Herrero Barbero, P., Martínez-Díaz, J. J., Álvarez-Gómez, J. A., Canora Catalán, C., and Insua Arévalo, J. M. (2018). "Tasas de acortamiento locales en el afloramiento de los Baños de Carralaca. Segmento Lorca-Totana de la Falla de Alhama de Murcia," in *Tercera reunión ibérica sobre fallas activas y paleosismología*. Editors C. Canora, F. Martín, E. Masana, R. Pérez, and M. Ortuño (Alicante (España), 95–98.
- Altunel, E., and Hancock, P. L. (1993a). Morphology and structural setting of quaternary travertines at pamukkale, Turkey. *Geol. J.* 28, 335–346. doi:10.1002/gj.3350280312
- Altunel, E., and Hancock, P. L. (1993b). "Active fissuring, faulting and travertine deposition at Pamukkale, Western Turkey," in *Neotectonics and active faulting*. Editors I. S. Stewart, C. Vita-Finzi, and L. A. Owen (kyoto, Japan: Zeitschrift für Geomorphologie), 285–302.
- Alvarez, F., Aldaya, F., and Navarro-Vilá, F. (1989). Miocene extensional deformation in the region of aguilas–mazarrón (eastern betic cordillera). *Estud. Geol.* 45, 369–374.
- Andrews, J. E. (2006). Palaeoclimatic records from stable isotopes in riverine tufas: Synthesis and review. *Earth-Science Rev.* 75, 85–104. doi:10.1016/j.earscirev.2005.08.002
- Arenas-Abad, C., Vázquez-Urbez, M., Pardo-Tirapu, G., and Sancho-Marcén, C. (2010). Fluvial and associated carbonate deposits. *Dev. Sedimentology* 61, 133–175.
- Argus, D. F., Gordon, R. G., DeMets, C., and Stein, S. (1989). Closure of the africa-urasia-north America plate motion circuit and tectonics of the gloria fault. *J. Geophys. Res.* 94, 5585–5602. doi:10.1029/jb094ib05p05585
- Armijo, R. (1977). La zona des failles Lorca–Totana (Cordillères Bétiques, Espagne). In *Etude tectonique et neotectonique, Thèse Illème cycle*. Paris: Univ. Paris VII.
- Ascione, A., Iannace, A., Imbriale, P., Santangelo, N., and Santo, A. (2013). Tufa and travertines of southern Italy: Deep-seated, fault-related CO₂ as the key control in precipitation. *Terra nova*. 26, 1–13. doi:10.1111/ter.12059
- Balanyá, J. C., and García-Dueñas, V. (1987). Les directions structurales dans le Domaine d'Alboran de part de d'autre du détroit de Gibraltar. *Compte Rendu Acad. Sci. Paris* 304, 929–933.
- Booth-Rea, G., Azañón, J. M., and Garci'a-Dueñas, V. C. (2004). Extensional tectonics in the northeastern Betics (SE Spain): Case study of extension in a multilayered upper crust with contrasting rheologies. *J. Struct. Geol.* 26, 2039–2058. doi:10.1016/j.jsg.2004.04.005
- Booth-Rea, G., Giaconia, F., and Martínez-Martínez, J. M. (2012). The Almenara detachment (southeastern Betics). *Geotemas* 16, 1615–1618.
- Booth-Rea, G., Ranero, C. R., Martínez-Martínez, J. M., and Grevemeyer, I. (2007). Crustal types and Tertiary tectonic evolution of the Alborán sea, Western Mediterranean. *Geochem. Geophys. Geosystems* 81.
- Broggi, A., Alçiçek, C., Yalçiner, C. C., Capezzuoli, E., Liotta, D., Meccheri, M., et al. (2016). Hydrothermal fluids circulation and travertine deposition in an active tectonic setting: Insights from the kamara geothermal area (Western anatolia, Turkey). *Tectonophysics* 680, 211–232. doi:10.1016/j.tecto.2016.05.003
- Broggi, A., Capezzuoli, E., Buracchi, E., and Branca, M. (2012). Tectonic control on travertine and calcareous tufa deposition in a low-temperature geothermal system (Sarteano, Central Italy). *J. Geol. Soc.* 169, 461–476. doi:10.1144/0016-76492011-137
- Broggi, A., Capezzuoli, E., Martini, I., Picozzi, M., and Sandrelli, F. (2014). Late quaternary tectonics in the inner northern apennines (siena basin, southern tuscany, Italy) and their seismotectonic implication. *J. Geodyn.* 76, 25–45. doi:10.1016/j.jog.2014.03.001
- Broggi, A., and Capezzuoli, E. (2009). Travertine deposition and faulting: the fault-Related travertine fissure ridge at terme S. Giovanni, rapolano terme (Italy). *Int. J. Earth Sci.* 98, 931–947. doi:10.1007/s00531-007-0290-z

wrote the first draft of the manuscript. All authors discussed the results and contributed to final version of the manuscript, including figure completion.

Funding

This research was funded by the Secretaría de Estado de Investigación, Desarrollo e Investigación (MINECO) project QUAKESTEP (CGL 2017-83931-C3-1-P) and Fundación Universidad Autónoma de Madrid (FUAM)-447820036-(L) Arcilla para el control medioambiental research line.

Conflict of interest

The authors declare that the research was conducted in the absence of any commercial or financial relationships that could be construed as a potential conflict of interest.

Publisher's note

All claims expressed in this article are solely those of the authors and do not necessarily represent those of their affiliated organizations, or those of the publisher, the editors and the reviewers. Any product that may be evaluated in this article, or claim that may be made by its manufacturer, is not guaranteed or endorsed by the publisher.

Supplementary material

The Supplementary Material for this article can be found online at: <https://www.frontiersin.org/articles/10.3389/feart.2023.1060363/full#supplementary-material>

- Burton, E. A., and Walter, L. M. (1987). Temperature or carbonate ion control? Relative precipitation rates of aragonite and Mg calcite from seawater. *Geology* 15, 111–114. doi:10.1130/0091-7613(1987)15<111:proaa>2.0.co;2
- Camuera, J., Alonso-Zarza, A. M., Rodríguez-Berriguete, A., and Rodríguez-González, A. (2014). Origin and palaeo-environmental significance of the berrazales carbonate spring deposit, north of gran canaria island, Spain. *Sediment. Geol.* 308, 32–43. doi:10.1016/j.sedgeo.2014.04.005
- Capezuoli, E., Gandin, A., and Pedley, M. (2014). Decoding tufa and travertine (fresh water carbonates) in the sedimentary record: The state of the art. *Sedimentology* 61, 1–21. doi:10.1111/sed.12075
- Caracausi, A., and Sulli, A. (2019). Outgassing of mantle volatiles in compressional tectonic regime away from volcanism: The role of continental delamination. *Geochem. Geophys. Geosystems* 20, 2007–2020. doi:10.1029/2018gc008046
- Cerón, J. C., Pulido Bosch, A., and Sanz de Galdeano, C. (1998). Isotopic identification of CO₂ from a deep origin in thermomineral waters of southeastern Spain. *Chem. Geol.* 149, 251–258. doi:10.1016/s0009-2541(98)00045-x
- Colak, E. S., Özkul, M., Aksoy, E., Kele, S., and Galheb, B. (2015). Travertine occurrences along major strike-slip fault zones: Structural, depositional and geochemical constraints from the Eastern Anatolian Fault System (EAFS), Turkey. *Geodin. Acta* 27, 154–173.
- Çolak, S., Aksoy, E., Koçyiğit, A., and İnceöz, M. (2012). The palu-uluova strike-slip basin in the east anatolian fault system, Turkey: Its transition from the palaeotectonic to neotectonic stage. *Turkish J. Earth Sci.* 21, 547–570. doi:10.3906/yer-1002-14
- Craig, H. (1961). Standard for reporting concentrations of deuterium and oxygen-18 in natural waters. *Science* 133, 1833–1834. doi:10.1126/science.133.3467.1833
- Crossey, L. J., Fischer, T. P., Patchett, P. J., Karlstrom, K. E., Hilton, D. R., Newell, D. L., et al. (2006). Dissected hydrologic system at the Grand Canyon; interaction between deeply derived fluids and plateau aquiferwaters in modern springs and travertine. *Geology* 34, 25–28. doi:10.1130/g22057.1
- Curewitz, D., and Karson, J. A. (1997). Structural settings of hydrothermal outflow: Fracture permeability maintained by fault propagation and interaction. *J. Volcanol. Geoth. Res.* 79, 149–168. doi:10.1016/s0377-0273(97)00027-9
- De Filippis, L., Faccenna, C., Billi, A., Anzalone, E., Brilli, M., Soligo, M., et al. (2013). Plateau versus fissure ridge travertines from Quaternary geothermal springs of Italy and Turkey: Interactions and feedbacks between fluid discharge, paleoclimate, and tectonics. *Earth-Science Rev.* 123, 35–52. doi:10.1016/j.earscirev.2013.04.004
- De Larouzière, F. D., Bolze, J., Bordet, P., Hernández, J., Montecat, C., and Ott d'Estevou, P. (1988). The Betic segment of the lithospheric Trans-Alboran shear zone during the Late Miocene. *Tectonophysics* 152, 41–52. doi:10.1016/0040-1951(88)90028-5
- De Pinho, R., Rodríguez-Berriguete, A., Alonso-Zarza, A., and Cabrera, M. (2015). The temisas carbonate building: An example of thermogene tufa system in gran canaria island. *Geogaceta* 57, 7–10.
- Dugamin, E. J. M., Richard, A., Cathelineau, M., Boiron, M. C., Despinos, F., and Brisset, A. (2021). Groundwater in sedimentary basins as potential lithium resource: A global prospective study. *Sci. Rep.* 11, 21091. doi:10.1038/s41598-021-99912-7
- Echeverría, A., Khazaradze, G., Asensio, E., Garate, J., Martín-Dávila, J., and Suriñach, E. (2013). Crustal deformation in eastern Turkey from CuaTeNeo GPS network. *Tectonophysics* 608, 600–612. doi:10.1016/j.tecto.2013.08.020
- Faccenna, C., Funicello, R., Montone, P., Parotto, M., and Voltaggio, M. (1993). Late Pleistocene strike slip tectonics in the acque albule basin (tivoli, latium). *Mem. Descr. della Carta Geol. d'Italia* 69, 37–50.
- Faccenna, C., Piromallo, C., Crespo-Blanc, A., Jolivet, L., and Rossetti, F. (2004). Lateral slab deformation and the origin of the Western Mediterranean arcs. *Tectonics* 23, 1–25. doi:10.1029/2002tc001488
- Faccenna, C., Soligo, M., Billi, A., De Filippis, L., Funicello, R., Rossetti, C., et al. (2008). Late Pleistocene depositional cycles of the Lapis Tiburtinus travertine (Tivoli, Central Italy): Possible influence of climate and fault activity. *Glob. Planet. Change* 63, 299–308. doi:10.1016/j.gloplacha.2008.06.006
- Fahad, M., and Saeed, S. (2018). Determination and estimation of magnesium content in the single phase magnesium-calcite [Ca(1-x)Mg_xCO₃(s)] using electron probe micro-analysis (EPMA) and X-ray diffraction (XRD). *Geosciences* 8, 303–312. doi:10.1007/s12303-017-0059-8
- Fernandes, R. M. S., Miranda, J. M., Meijninger, B. M. L., Bos, M. S., Noomen, R., Bastos, L., et al. (2007). Surface velocity field of the Ibero-Maghrebian segment of the Eurasia-Nubia plate boundary. *Geophys. J. Int.* 169, 315–324. doi:10.1111/j.1365-246x.2006.03252.x
- Ferrater, M., Ortuño, M., Masana, E., Pallás, R., Perea, H., Baize, S., et al. (2016). Refining seismic parameters in low seismicity areas by 3D trenching: The Alhama de Murcia fault, SE Iberia. *Tectonophysics* 680, 122–128. doi:10.1016/j.tecto.2016.05.020
- Ferrater, M., Ortuño, M., TeresaMasana, E., Martínez Díaz, J. J., Pallas, R., Peea, H., et al. (2017). Lateral slip rate of Alhama de Murcia fault (SE Iberian Peninsula) based on a morphotectonic analysis: Comparison with paleoseismological data. *Quat. Int.* 451, 87–100. doi:10.1016/j.quaint.2017.02.018
- Filiz, S. (1984). "Investigation of the important geothermal areas by using C, H, O isotopes," in *Seminar on the utilization of geothermal Energy for electric power generation and space heating* (Florence, Italy, 14–17).
- Fouke, B. W., Farmer, J. D., Des Marais, D. J., Pratt, L., Sturchio, N. C., Burns, P. C., et al. (2000). Depositional facies and aqueous-solid geochemistry of travertine depositing hot springs (Angel Terrace, Mammoth Hot Springs, Yellowstone National Park, U.S.A.). *J. Sediment. Res.* 70, 565–585. doi:10.1306/2dc40929-0e47-11d7-8643000102c1865d
- Friedman, I. (1970). Some investigations of the deposition of travertine from Hot Springs—I. The isotopic chemistry of a travertine-depositing spring. *Geochimica Cosmochimica Acta* 34, 1303–1315. doi:10.1016/0016-7037(70)90043-8
- Gilli, E. (2005). Review on the use of natural cave speleothems as palaeoseismic or neotectonics indicators. *Comptes Rendus Geosci.* 337, 1208–1215. doi:10.1016/j.crte.2005.05.008
- Giwell, A., Esteban, L., Delle Piane, C., and Clennell, M. B. (2016). Fault reactivation in travertine and its impact on hydraulic transmissibility: laboratory experiments and mesoscale structures. *Pet. Geosci.* 23, 92–103. doi:10.1144/petgeo2016-025
- Gómez-Novell, O. (2021). *Paleoseismic transect across the Alhama de Murcia Fault and implications of a fault-based seismic hazard assessment for the Eastern Betics*. doi:10.13140/RG.2.2.28807.11685/2
- Gradziński, M., Wroblewski, W., Dulinski, M., and Hercman, H. (2014). Earthquake-affected development of a travertine ridge. *Sedimentology* 61, 238–263. doi:10.1111/sed.12086
- Hancock, P. L., Chalmers, R. M. L., Altunel, E., and Çakır, Z. (1999). Travertines: using travertines in active fault studies. *J. Struct. Geol.* 21, 903–916. doi:10.1016/s0191-8141(99)00061-9
- Herrero Barbero, P., Álvarez Gómez, J. A., and Martínez Díaz, J. J. (2017). Análisis estructural en el segmento Alhama de Murcia – Alcántarilla (Falla de Alhama de Murcia) y sus implicaciones en la peligrosidad sísmica. *Geogaceta* 62, 11–14.
- Herrero Barbero, P., Álvarez Gómez, J. A., Martínez Díaz, J. J., and Klimowitz, J. (2020). Neogene basin inversion and recent slip rate distribution of the northern termination of the Alhama de Murcia Fault (Eastern Betic Shear Zone, SE Spain). *Tectonics* 39. doi:10.1029/2019TC005750
- Kele, S., Breitenbach, S. F. M., Capezuoli, E., Nele Meckler, A., Ziegler, M., Millan, I. M., et al. (2015). Temperature dependence of oxygenated clumped isotope fractionation in carbonates: a study of travertines and tufas in the 6–95°C temperature range. *Geochimica Cosmochimica Acta* 168, 172–192. doi:10.1016/j.gca.2015.06.032
- Kele, S., Ozkul, M., Gokgoz, A., Forizs, I., Baykara, M. O., Alciçek, M. C., et al. (2011). Stable isotope geochemical study of Pamukkale travertines: New evidences of low-temperature non-equilibrium calcite-water fractionation. *Sediment. Geol.* 238, 191–212. doi:10.1016/j.sedgeo.2011.04.015
- Loneragan, L., and Schreiber, B. C. (1993). Proximal deposits at a fault-controlled basin margin, Upper Miocene, SE Spain. *J. Geol. Soc. Lond.* 150, 719–727. doi:10.1144/gsjgs.150.4.0719
- Loneragan, L., and White, N. (1997). Origin of the Betic-Rif mountain belt. *Tectonics* 16, 504–522. doi:10.1029/96tc03937
- Malone, M. J., and Baker, P. (1999). Temperature dependence of the strontium distribution coefficient in calcite: An experimental study from 400c to 200c and application to Natural diagenetic calcites. *J. Sediment. Res.* 69, 216–223. doi:10.2110/jsr.69.216
- Manfra, L., Masi, U., and Turi, B. (1974). Effetti isotopici nella diagenesi dei travertini. *Geol. Romana* 13, 147–155.
- Martí, A., Queralt, P., Ledo, J. J., Marcuello, A., Álvarez-Aramberri, J., and Martínez-Díaz, J. J. (2016). "Magnetotelluric characterization of the Alhama de Murcia Fault (Eastern Betics): Preliminary results," in *Proceedings, near surface geoscience-22nd European meeting of environmental and engineering Geophysics* (Barcelona, Spain–29500161).
- Martínez, M., and Moreno, L. (2005). Los balnearios olvidados y las salinas de interior de la Región de Murcia: Un patrimonio hidrogeológico a redescubrir y su aplicación a la didáctica geológica. *Enseñanza las Ciencias Tierra* 13 (2), 177–184.
- Martínez-Díaz, J. J., Alonso-Henar, J., Insua-Arévalo, J. M., Canora, C., García-Mayordomo, J., Rodríguez-Escudero, E., et al. (2018). Geological evidences of surface rupture related to a seventeenth century destructive earthquake in Betic Cordillera (SE Spain): Constraining the seismic hazard of the Alhama de Murcia fault. *J. Iber. Geol.* 45, 73–86. doi:10.1007/s41513-018-0082-2
- Martínez-Díaz, J. J., and Hernández-Enrile, J. (2001). Using travertine deformations to characterize paleoseismic activity along an active oblique-slip fault: The Alhama de Murcia fault (Betic Cordillera, Spain). *Acta Geol. hispánica* 36, 3–4.
- Martínez-Díaz, J. J., Masana, E., Hernández-Enrile, J. L., and Santanach, P. (2003). Effects of repeated paleoearthquakes on the Alhama de Murcia fault (Betic Cordillera, Spain) on the Quaternary evolution of an alluvial fan system. *Ann. Geophys.* 46, 775–792.
- Martínez-Díaz, J. J., Masana, E., and Ortuño, M. (2012). Active tectonics of the Alhama de Murcia fault, Betic Cordillera, Spain. *J. Iber. Geol.* 38, 253–270. doi:10.5209/rev_jige.2012.v38.n1.39218
- Martínez-Martínez, J. M., and Azañón, J. M. (1997). Mode of extensional tectonics in the southeastern Betics (SE Spain): Implications for the tectonic evolution of the peri-Alborán orogenic system. *Tectonics* 16, 205–225. doi:10.1029/97tc00157
- Martí 'nez-Dí 'az, J. J. (2002). Stress field variation related to fault interaction in a reverse oblique-slip fault: the Alhama de Murcia fault, Betic Cordillera, Spain. *Tectonophysics* 356, 291–305. doi:10.1016/s0040-1951(02)00400-6
- Masana, E., Martínez-Díaz, J. J., Hernández-Enrile, J. L., and Santanach, P. (2004). The Alhama de Murcia fault (SE Spain), a seismogenic fault in a diffuse plate boundary.

- Seismotectonic implications for the Ibero-Magrebien region. *J. Geophys. Res.* 109, 1–17. doi:10.1029/2002jb002359
- Masona, J., Schneiderwinda, S., Pallikarakis, A., Mechernich, S., Papanikolaou, I., and Reicherter, K. (2017). Hanging-wall colluvial cementation along active normal faults. *Quat. Res.* 88, 39–59. doi:10.1017/qua.2017.32
- Meijninger, B. M. L., and Vissers, R. L. M. (2006). Miocene extensional basin development in the Betic Cordillera, SE Spain revealed through analysis of the Alhama de Murcia and Crevillente Faults. *Basin Res.* 18, 547–571. doi:10.1111/j.1365-2117.2006.00308.x
- Minissale, A., Kerrick, D. M., Magro, G., Murrell, M. T., Paladini, M., Rihs, S., et al. (2002). Geochemistry of Quaternary travertines in the region north of Rome (Italy): structural, hydrologic and paleoclimatic implications. *Earth Planet. Sci. Lett.* 203, 709–728. doi:10.1016/s0012-821x(02)00875-0
- Montenat, C. (1973). *Les formations néogènes du Levant espagnol*. Ph.D. Thesis. Orsay, France: University of Paris.
- Newell, D. L., Crossey, L. J., Karlstrom, K., Fischer, T., and Hilton, D. (2005). Continental-scale links between the mantle and groundwater systems of the Western United States: Evidence from travertine springs and regional He isotope data. *GSA Today* 15, 4–10. doi:10.1130/1052-5173(2005)015<4:csbltm>2.0.co;2
- Ortuño, M., Masana, E., García-Meléndez, E., Martínez-Díaz, J. J., Štěpančíková, P., Cunha, P., et al. (2012). An exceptionally long paleoseismic record of a slow-moving fault: the Alhama de Murcia fault (Eastern Betic Shear Zone, Spain). *Geol. Soc. Am. Bull.* 124, 1474–1494. doi:10.1130/b30558.1
- Özkul, M., Gökgöz, A., Kele, S., Baykara, M. O., Shen, C.-C., Chang, Y.-W., et al. (2014). Sedimentological and geochemical characteristics of a fluvial travertine: A case from the eastern Mediterranean region. *Sedimentology* 61, 291–318. doi:10.1111/sed.12095
- Özkul, M., Kele, S., Gökgöz, A., Shen, C., Jones, B., Baykara, M. O., et al. (2013). Comparison of the Quaternary travertine sites in the Denizli extensional basin based on their depositional and geochemical data. *Sediment. Geol.* 294, 179–204. doi:10.1016/j.sedgeo.2013.05.018
- Pedley, H. M. (2009). Tufas and travertines of the Mediterranean region: a testing ground for freshwater carbonate concepts and developments. *Sedimentology* 56, 221–246. doi:10.1111/j.1365-3091.2008.01012.x
- Pentecost, A. (2005). *Travertine*. Berlin: Springer-Verlag, 446.
- Rodrigo-Naharro, J., Delgado, A., Herrero, M. J., Granados, A., and Pérez del Villar, L. (2013). Current Travertines Precipitation from CO₂-rich Groundwaters as an alert of CO₂ Leakages from a Natural CO₂ Storage at Gañuelas-Mazarrón Tertiary Basin (Murcia, Spain). *Inf. Técnicos Ciemat* 1279, 54.
- Rodríguez-Escudero, E., Martínez-Díaz, J. J., Giner-Robles, J. L., Tsige, M., and Cuevas-Rodríguez, J. (2020). Pulverized quartz clasts in gouge of the Alhama de Murcia fault (Spain): Evidence for coseismic clast pulverization in a matrix deformed by frictional sliding. *Geology* 48, 283–287. doi:10.1130/g47007.1
- Rodríguez-Fernández, J., Azor, A., and Azañón, J. M. (2012). “The Betic intramontane basins (SE Spain): Stratigraphy, subsidence, and tectonic history,” in *Tectonics of sedimentary basins. Recent advances*. Editors C. Busby and A. Azor, 23, 461–479.
- Sanjuan, B., Gourcerol, B., Millot, R., Rettenmaier, D., Jeandel, E., and Rombaut, A. (2022). Lithium-rich geothermal brines in Europe: An up-date about geochemical characteristics and implications for potential Li resources. *Geothermics* 101, 102385. doi:10.1016/j.geothermics.2022.102385
- Selim, H. H., Yavuz, O., Güner, Ö., Karakaş, A., and Taş, K. (2016). Age determination for segments of the North Anatolian Fault (NAF) northern branch by ²³⁴U/²³⁰Th dating of Soğucak (Yalova) range-front travertines, south Marmara, Turkey. *Quat. Int.* 425, 416–424. doi:10.1016/j.quaint.2016.08.035
- Serpelloni, E., Vannucci, G., Pondrelli, S., Argnani, A., Casula, G., Anzidei, M., et al. (2007). Kinematics of the Western Africa-Eurasia plate boundary from focal mechanisms and GPS data. *Geophys. J. Int.* 169, 1180–1200. doi:10.1111/j.1365-246x.2007.03367.x
- Shi, Z., Shi, Z., Yinc, G., and Liang, J. (2014). Travertine deposits, deep thermal metamorphism and tectonic activity in the Longmenshan tectonic region, southwestern China. *Tectonophysics* 633, 156–163. doi:10.1016/j.tecto.2014.06.020
- Shi, Z., ShiYin, G., and Liang, J. (2014). Travertine deposits, deep thermal metamorphism and tectonic activity in the Longmenshan tectonic region, southwestern China. *Tectonophysics* 633, 156–163. doi:10.1016/j.tecto.2014.06.020
- Sibson, R. H. (1990). *Conditions for fault-valve behavior*. Geological Society, 54. London: Special Publications, 15–28.
- Sibson, R. H. (2004). “Frictional mechanics of seismogenic thrust systems in the upper continental crust. Implications for fluid overpressures and redistribution,” in *Thrust tectonics and hydrocarbon systems*. Editor K. R. McClay (London: AAPG Memoir), 82, 1–17.
- Sibson, R. H. (1996). Structural permeability of fluid-driven fault–fracture meshes. *J. Struct. Geol.* 18, 1031–1042. doi:10.1016/0191-8141(96)00032-6
- Silva, P. G. (1994). *Evolución geodinámica de la Depresión del Guadalentín desde el Mioceno Superior hasta la actualidad: Neotectónica y Geomorfología (Doctoral Thesis)*. Madrid: Universidad Complutense de Madrid.
- Silva, P. G., Goy, J. L., Zazo, C., Lario, J., and Bardají, T. (1997). Paleoseismic indications along ‘aseismic’ fault segments in the Guadalentín Depression (SE Spain). *J. Geodyn.* 24, 105–115. doi:10.1016/s0264-3707(97)00011-2
- Silva, P. G., Harvey, A. M., Zazo, C., and Goy, J. L. (1992). Geomorphology, depositional style and morphometric relationships of Quaternary alluvial fans in the Guadalentín Depression (Murcia, southeast Spain). *Z. für Geomorphol.* 36, 325–341. doi:10.1127/zfzg/36/1992/325
- Spötl, C., Mangini, A., Frank, N., Eichstädter, R., and Burns, S. (2002). Start of the last interglacial period at 135 ka: Evidence from a high Alpine speleothem. *Geology* 30, 815–818. doi:10.1130/0091-7613(2002)030<0815:sotlip>2.0.co;2
- Stanienda Pilecki, K. J. (2018). Magnesium calcite in Muschelkalk limestones of the Polish part of the Germanic Basin. *Carbonates Evaporites* 33, 801–821. doi:10.1007/s13146-018-0437-y
- Temiz, U., and Eikenberg, J. (2011). U/Th dating of the travertine deposited at transfer zone between two normal faults and their neotectonic significance: Cambazlı fissure ridge travertines (the Gediz Graben e Turkey). *Geodin. Acta* 24, 95–105.
- Temiz, U., Gokten, Y. E., and Eikenberg, J. (2013). Strike-slip deformation and U/Th dating of travertine deposition: Examples from North Anatolian Fault Zone, Bolu and Yenicag Basins, Turkey. *Quat. Int.* 312, 132–140. doi:10.1016/j.quaint.2013.08.034
- Turi, B. (1986). “Stable isotope geochemistry of travertines,” in *In handbook of environmental isotope geochemistry*. Editors B. P. Fritz and J. C. Fontes (Amsterdam: Elsevier), 207–238.
- Uysal, İ. T., Feng, Y., Zhao, J., Isik, V., Nuriel, P., and Golding, S. (2009). Hydrothermal CO₂ degassing in seismically active zones during the late Quaternary. *Chem. Geol.* 265, 442–454. doi:10.1016/j.chemgeo.2009.05.011
- Uysal, T., Feng, Y., Zhao, J. X., Altunel, E., Weatherley, D., Karabacak, V., et al. (2007). U-series dating and geochemical tracing of late Quaternary travertine in co-seismic fissures. *Earth Planet. Sci. Lett.* 257, 450–462. doi:10.1016/j.epsl.2007.03.004
- Vignaroli, G., Berardi, G., Billi, A., Kele, S., Rossetti, F., Soligo, M., et al. (2016). Tectonics, hydrothermalism, and paleoclimate recorded by Quaternary travertines and their spatio-temporal distribution in the Albegna basin, central Italy: Insights on Tyrrhenian margin neotectonics. *Lithosphere* 8, 335–358. doi:10.1130/l507.1
- Wang, H., Yang, G., Qin, J. M., Guo, J. Q., and Cao, J. (2007). Records of Paleoclimate changes based on the Dawanzhangjiagou travertine deposition profile in Huanglong, Sichuan (in Chinese with English abstract). *Acta Geosci. Sin.* 28, 469–474.
- Zentmyer, R., Myrow, P., and Newell, D. (2008). Travertine deposits from along the South Tibetan Fault System near Nyalam, Tibet. *Geol. Mag.* 145, 753–765. doi:10.1017/s0016756808005323
- Zhang, F., Xu, H., Konishi, H., and Roden, E. E. (2010). A relationship between d104 value and composition in the calcite-disordered dolomite solid-solution series. *Am. Mineralogist* 95, 1650–1656. doi:10.2138/am.2010.3414
- Zhou, G. T., and Zheng, Y. F. (2006). On the direction and magnitude of oxygen isotope fractionation between calcite and aragonite at thermodynamic equilibrium. *Aquat. Geochem.* 12, 239–268. doi:10.1007/s10498-005-5857-3